# Chapter 1

# Photochemistry in $H_2O$:$CO_2$:$NH_3$:$CH_4$ ice mixtures

Photochemistry in $NH_3$-containing ices provides a pathway to forming amino acids and other prebiotically interesting molecules during star formation. Quantifying the UV induced ice chemistry *in situ* has so far failed for realistic astrophysical ice analogues because of a multitude of photoproducts with overlapping infrared spectral features. While such an analogue is included in this study, the focus is instead on the spectroscopic quantification of the photochemistry at 20 K in a number of simpler ices with $H_2O$, $CO_2$, $NH_3$ and/or $CH_4$ to acquire a general understanding of branching ratios and diffusion of radicals in ices. The production of $C_2H_6$, $C_2H_4$, $N_2H_4$, CO, $CO_3$, $O_3$, $CH_3NH_2$, HCN, $CH_3OH$, $H_2CO$, $CH_3CH_2OH$, $CH_3CHO$ and $OCN^-$ are quantified during UV irradiation, revealing a clear difference between species that form directly from reactions between first generation radicals and from later generation products. From the different formation rates of $C_2H_6$ and $C_2H_4$, the contested $CH_4$ photodissociation $CH_3$:$CH_2$ branching ratio is 3:1. The photochemistry in $H_2O$-poor and $H_2O$-rich ices differs because of the stronger binding environment in $H_2O$-rich ices, which increases the importance of relative diffusion barriers of radicals. Acid-base chemistry is important in all $NH_3$:$CO_2$ containing ices; it increases the effective photodestruction cross section of $NH_3$ ice by up to an order of magnitude because of proton transfer from other photoproducts. Acid-base chemistry also increases the product desorption temperatures. Finally TPD experiments following irradiation are presented for the first time, which confirms that amino acids and amino acid-like molecules form during photolysis of ices with $CH_4$, $NH_3$ and $CO_2$. A larger model together with new experiments at different temperatures are needed to further constrain different diffusion barriers and thus to model the cproduction of complex molecules, including amino acids, in space.

[0]Öberg et al. in preparation

## 1.1 Introduction

The molecules of life, DNA, RNA and proteins, are built up from amino acids and sugars. Pre-biotic production pathways of sugars and different nitrogen-bearing organic molecules are thus of considerable interest and a necessary component of different origin-of-life scenarios. The recent discovery of $CH_3CH_2OCHO$ and $C_3H_7CN$ towards Sagittarius B2(N) is indicative of an efficient formation pathway to organic molecules of comparable complexity to the smallest amino acids during the early stages of star formation (Belloche et al. 2009). Laboratory and model efforts suggest that ice photochemistry on dust-grains during the protostellar stage produces carbon- and oxygen-containing complex molecules with high enough efficiency to explain the observed abundances (e.g. Muñoz Caro et al. 2002; Garrod & Herbst 2006; Garrod et al. 2008; Belloche et al. 2009, Chapter 10).

The ice-covered grains from the protostellar stage eventually become incorporated into the protoplanetary disk and there they collide and agglomerate to form larger and larger grains and eventually boulders and planetesimals. If the protostellar ices survive this stage, as suggested by models of Visser et al. (2009), the formed meteorites and comets may subsequently enrich planets with complex organic molecules. The importance of this last stage for the prebiotic chemistry on planets depends on the ice chemistry proceeding planet formation and this chapter aims to quantify the formation of nitrogen-containing complex molecules in a large set of ice-mixtures of astrophysical interest and thus deduce the necessary conditions to produce amino acids and other pre-biotically interesting molecules during star- and planet-formation.

Simple ices form in molecular clouds through hydrogenation and oxygenation of atoms and unsaturated molecules. Observations of ices before the onset of star formation reveal $H_2O$ ice to be the main constituent, followed by CO and $CO_2$ (e.g. Whittet et al. 1998; Bergin et al. 2002). $CH_4$ and $NH_3$ ice probably form before the protostellar stage as well, but have only been detected around protostars (Gibb et al. 2004; Knez et al. 2005, Chapter 2). $NH_3$ is the main ice-carrier of nitrogen that is directly observed; $N_2$ may be present, but has no strong infrared transitions and CN-bearing species have an order of magnitude lower abundance (van Broekhuizen et al. 2005). $NH_3$ ice was first discovered by Lacy et al. (1998) and is now established to exist at abundances of 5–10% with respect to $H_2O$ ice towards both high-mass and low-mass protostars (Gibb et al. 2004, Bottinelli et al. in prep). From the $NH_3$ ice spectral profile and its proposed formation pathway through hydrogenation of nitrogen, $NH_3$ should form in the $H_2O$-rich ice layer. This ice phase also contains 20–30% $CO_2$ and ∼5% $CH_4$. In contrast $CH_3OH$ ice

probably forms in a CO-rich ice layer frozen out on top of the $H_2O$-rich ice.

Organic nitrogen-containing molecules have been detected in the gas phase in the hot regions close to protostars, in galactic center clouds, in a low-mass outflow and in cometary outflows (see Herbst & van Dishoeck, 2009 for review). The most abundant species are HCN, $CH_3CN$ and HNCO, but the recently discovered $C_3H_7CN$ and $NH_2CH_2CN$ have been detected with relatively high fractional abundances with respect to $H_2$, $1.0 \times 10^{-9}$ and $2.2 \times 10^{-9}$, respectively (Belloche et al. 2008, 2009).

Towards a sample of high-mass protostellar hot cores the four nitrogen containing organic molecules searched for, HNCO, $CH_3CN$, $C_2H_5CN$ and $NH_2CHO$, were all detected to have high rotational temperatures, while CHO-containing molecules without nitrogen could be divided into two temperature bins, tracing the hot core and the luke-warm envelope, respectively (Bisschop et al. 2007b). The high temperature of the nitrogen-bearing species is consistent with their formation and trapping in the $H_2O$-rich ice, while CHO-containing species forming in the CO-rich outer ice layer are more exposed and thus desorb easier because of heat and non-thermal desorption pathways. The abundances of nitrogen bearing complex molecules and of the other detected complex species are also not correlated between sources, again consistent with the formation of nitrogen containing and CHO-containing complex molecules in different phases of the ice. The CHO-containing complex species then depend on the original $CH_3OH$ content (Chapter 10), while the N-containing species do not.

Some complex nitrogen-bearing molecules have been detected in comets as well, including HNCO and $CH_3CN$ (Altwegg et al. 1999; Crovisier et al. 2004). The simplest amino acid is yet undetected towards both comets and star-forming regions despite deep searches. The current abundance upper limits are $\sim 10^{-11}$ with respect to hydrogen in the Orion star forming region, and $1 \times 10^{-10}$ in the cold envelope and $7 \times 10^{-9}$ in the hot core of the solar-type protostar IRAS 16293-2422 (Combes et al. 1996; Ceccarelli et al. 2000). Amino acids are however found in meteorites where more sensitive analysis methods are available, but the detected acids may form when meteoric pre-cursors comes in contact with $H_2O$ during the analysis (Engel & Macko 1997).

The photochemistry of $NH_3$ containing ices was first investigated for astrophysically relevant ice mixtures by Hagen et al. (1979), who irradiated a $CO{:}H_2O{:}NH_3{:}CO_2$ 50:1:1:0.09 ice at ~10 K with a UV lamp peaking at 160 nm. HNCO, $H_2CO$, $NH_2CHO$ and HCOOH were identified among the products and unidentified large molecules with molecular masses up to 514 were recorded mass-spectrometrically following warm-up to room temperatures of the

photolyzed ice residue. There is thus qualitative evidence for a nitrogen-based complex chemistry upon irradiation of $NH_3$-containing ice mixtures. Other early experimental studies investigated the qualitative effects of adding different species to the mixtures and changing the original abundance ratios (e.g. Allamandola et al. 1988; Grim et al. 1989; Schutte et al. 1993). Two of the main results were the relative ease at which XCN compounds, especially $OCN^-$, form in different $NH_3$ containing ices and also that moderately complex $NH_2$-containing molecules form, which may be amino acid pre-cursors. The largest infrared detected molecule is $C_6H_{12}N_4$ Bernstein et al. (1995); Muñoz Caro & Schutte (2003).

These experiments were all carried out under high-vacuum conditions, where thick ices (tens of $\mu$m) were deposited at ~10 K while irradiating the ice to produce the maximum amount of radicals. The photolyzed ices were then heated to room temperature and the residue analyzed mass-spectrometrically. These conditions were necessary when carrying out experiments under high-vacuum and employing transmission spectroscopy. It is however difficult to deduce from these experiments what molecules will form under interstellar conditions and at what abundances. Specifically, none of these studies provide any quantitative data on reaction rates of nitrogen-containing molecules. They thus do not present data that can be included in astrochemical models to test whether ice photochemistry produces the correct amounts and correct abundance ratios of complex molecules, under interstellar conditions and timescales, compared to astrophysical observations. Still it is encouraging that the experiments produced several of the molecules observed towards protostars. The early studies also provided some conceptual understanding of the processes involved, i.e. photodissociation followed by radical diffusion, to produce the observed products.

Bernstein et al. (2002) and Muñoz Caro et al. (2002) first reported on efficient amino acid production, in similar high-vacuum experiments, following irradiation of ices; the amino acids were detected using gas chromatography and mass spectrometry of the irradiated ice residue after the sample was heated to room temperature. These studies were followed up with both models and isotopically labelled experiments to constrain the formation mechanisms (Woon 2002; Muñoz Caro et al. 2004; Elsila et al. 2007; Nuevo et al. 2007; Lee et al. 2009). The general conclusion is that amino acids form through a variety of radical-radical reactions and while it is more efficient in a HCN-containing matrix, pathways from $NH_3$ exist as well. It is however still unclear when these amino acids form, i.e. if there is a cold formation pathway or if heating to room temperature is required.

Overall these experimental results are enticing since they suggest that amino acid production may be possible in interstellar ices. Final yields in a laboratory

setting provide little information about what the final fraction will be under different astrophysical conditions, however – the reported carbon-conversion efficiencies, up to 0.5%, may be a result of the experimental technique where thick ice samples are deposited during irradiation, which probably over-produces radicals. Under astrophysical conditions, where the time scales are orders of magnitudes longer, the chemistry may take a very different turn indeed and this can only be investigated if the fundamental physical quantities governing ice chemistry are understood, i.e. photodissociation cross sections, diffusion barriers and reaction barriers of different molecules and radicals.

Despite a lack of this kind of data, a complex nitrogen chemistry was incorporated in a recent grain-gas model of the complex ice chemistry in protostellar envelopes and subsequent desorption in the hot core close to the protostar (Garrod et al. 2008). The model assumes a perfectly mixed ice, which probably explains why it over-produces $NH_2CHO$, but under-produces $CH_3CN$ and $CH_3NH_2$; if $NH_3$ is mainly formed in the $H_2O$-rich layer it will have more access to $CH_4$-dissociation products than to CO-reaction products. Model improvements are mainly limited by the lack of quantitative data on the $NH_3$ ice photochemistry.

Such quantitative data should be possible to derive from simpler binary ice mixtures, since e.g. the $CH_3$ diffusion barrier in any $H_2O$ dominated ice should be approximately the same. Reaction barriers only depend on the two radicals reacting and while effective photodissociation cross-sections may change with temperature or ice mixture because of changing diffusion barriers (Chapter 10), the branching ratio should solely depend on the UV lamp spectrum. Quantifying the complex ice chemistry of astrophysically relevant ice mixtures should thus be possible through a combined approach where physical quantities are extracted from simple, well-constrained ice mixtures followed by a few experiments on more complicated mixtures to ensure that these results are consistent with predictions from the simpler ice experiments.

This chapter presents the production of moderately complex species, up to glycine, in a large set of ice mixtures during irradiation at 20 K and during warm-up between 20 and 200 K. In difference to most previous experiments the irradiation is done after deposition and the complex molecule formation is followed *in situ* using infrared spectroscopy and temperature programmed desorption (TPD). The main part of the chapter focuses on the photodesorption, photodissociation and product formation during irradiation of pure and binary ices. Section 1.3.2 then presents the quantification of the same products in more complicated mixtures together with TPD experiments following irradiation of an astrophysical ice analogue and five other mixtures, which are used for comparison, to identify the

most complex photoproducts accesible for *in situ* study. The results are used in the Discussion section to constrain photodissociation branching ratios, relative diffusion barriers and the reaction pathways that the observed molecules form through. The implications for understanding ice chemistry in an astrophysical setting is discussed, followed by proposed new experiments to further constrain the chemistry and some concluding remarks.

## 1.2 Experimental

All experiments are carried out on the set-up CRYOPAD under ultra-high vacuum conditions ($\sim 10^{-9}$–$10^{-10}$ mbar). Pure and mixed ices are deposited diffusively at 18 K by introducing a gas (mixture) in the vacuum chamber along the surface normal of a gold substrate, which is temperature controlled down to 18 K with a 2 K uncertainty. The gas mixtures of 10–20 mbar are prepared in a separate glass manifold with a base pressure of $10^{-4}$ mbar. The $CO_2$, $NH_3$ and $CH_4$ gases have a minimum purity of 99.9% (Indugas). Samples containing $H_2O$ are prepared from the vapour pressure of deionised $H_2O$, further purified through several freeze-thaw cycles.

The ices are probed through infrared spectroscopy in Reflection-Absorption mode (RAIRS) and the desorbed molecules during warm-up are investigated with a Quadropole Mass Spectrometer (QMS), placed in front of the substrate. As described in Chapters 8–10 relative RAIRS band strengths are consistent with relative transmission band strengths and thus certain within 20–30%. Absolute band strengths have a 50% uncertainty, but this only affects the derived photodesorption rates – not the quantification of the chemistry.

The original ice mixture as well as the changes induced by UV irradiation in the ice composition are quantified using RAIRS, while the QMS is employed to secure band identifications of photoproducts. The UV irradiation is provided by a hydrogen-discharge lamp with UV emission around Ly-$\alpha$ and through a broader continuum between 6 and 11.5 eV. All ices are irradiated with a UV flux of $1.1(\pm 0.4)\times 10^{13}$ s$^{-1}$ cm$^{-2}$ except for experiment aimed to determine the photodesorption yield (Exp. 1), where a four times higher flux is used. Following irradiation the photolysed ices are heated by 1 K min$^{-1}$ in TPD experiments, while monitoring a range of mass signals between 2 and 62 with the QMS.

Table 1.1 lists the photochemistry experiments in terms of their mixture composition and total thickness. The set of experiments have been designed to test the influence of different combinations of $H_2O$, $CO_2$, $NH_3$ and $CH_4$ on the complex product formation. Experiment 18 was chosen to mimic the $H_2O$-rich phase

Table 1.1. The compositions and thickness of the photochemistry experiments.

| Exp. | $H_2O$ | $CO_2$ | $CH_4$ | $NH_3$ | Thickness (ML) | $\phi^a(10^{-18}cm^2)$ |
|---|---|---|---|---|---|---|
| 1 | | | | 1 | 8 | |
| 2 | | | | 1 | 51 | 1.5±0.5 |
| 3 | 1 | | | | 43 | |
| 4 | | 1 | | | 15 | |
| 5 | | | 1 | | 47 | |
| 6 | 1 | | | 1 | 54 | 1.7±0.6 |
| 7 | 4 | | | 1 | 43 | 5.6±2.0 |
| 8 | | 1 | | 2.5 | 44 | 5.7±2.0 |
| 9 | | | 3 | 2 | 45 | 2.2±0.8 |
| 10 | 1 | 1.5 | | | 21 | |
| 11 | 6 | 1 | | | 35 | |
| 12 | 1 | | 3 | | 42 | |
| 13 | 2 | | 1 | | 37 | |
| 14 | | 1 | 2 | | 33 | |
| 15 | 1 | 1 | | 1 | 69 | |
| 16 | 1 | | 1 | 1 | 66 | |
| 17 | | 1 | 1 | 1 | 78 | |
| 18 | 100 | 20 | 8 | 12 | 66 | |

[a]The initial $NH_3$ Photodestruction cross-section

observed towards low-mass protostars (Chapter 2). All experiments are irradiated at 20 K followed by warm-up by 1 K $min^{-1}$ to 150–250 K, while acquiring RAIRS every 10 min and monitoring the desorption products with the QMS. The ice thicknesses range between ~8–78 monolayers (ML). This ice thickness regime is similar to what is expected in the dense and cold stages of star formation. Each ice in experiment 2–18 was irradiated for 6 hours, resulting in a UV fluence of $\sim 2.3 \times 10^{17}$ $cm^{-2}$. This is comparable to the fluence an ice in a cloud core is exposed to during $10^6$ years because of cosmic-ray induced UV photons at a flux of $10^4$ $cm^{-2}$ (Shen et al. 2004).

## 1.3 Results

The results are divided into two main sections, presenting first the photochemistry in pure ices and in binary mixtures and second in astrophysical ice analogues with three or four components. In both cases the starting material is $H_2O$, $CO_2$, $NH_3$ and $CH_4$ ices in different combinations and mixture ratios. The chemistry of the binary and pure ices is quantified based on RAIR spectra acquired during irradiation and warm-up. The focus is on quantifying a number of well understood infrared bands that can be assigned to photoproducts up to $CH_3CH_2OH$ and $OCN^-$ in size, rather than identifying all possible photoproducts. This is in line with the aim of the chapter to derive quantities such as diffusion barriers rather than determining the complete complex chemistry in a laboratory setting.

Quantification through infrared spectroscopy is only possible for a few of the photoproducts in the more complex ice mixtures because of a multitude of photoproducts with overlapping infrared features. Therefore the tertiary and four-component ice mixtures are also investigated using TPD experiments to test whether larger molecules, predicted from the binary ice mixture chemistry, form in these ices.

### 1.3.1 Photochemistry in binary ice mixtures

The initial ice compositions, and the photodesorption and photodissociation yields are also calculated from the listed ice bands in Table 1.2. Table 1.2 also lists the photoproducts considered in this section, together with the infrared bands used for quantification, transmission band strengths and literature references on the ice spectra. Most photoproduct bands are easily identified from their spectral positions alone, but a few bands required further analysis to securely assign to a specific complex species.

Table 1.2 The original ice infrared bands and the photoproduct spectral features used for quantification.

| Species | Band ($cm^{-1}$) | Band strength[a] ($cm^{-1}$) | Reference |
|---|---|---|---|
| $CH_4$ | 1300 | $6.1\times10^{-18}$ | Moore & Hudson (1998) |
| $NH_3$ | 1070 | $1.7\times10^{-17}$ | D'Hendecourt & Allamandola (1986) |
| $CO_2$ | 2343 | $7.6\times10^{-17}$ | Gerakines et al. (1995) |
| $H_2O$ | 1670 | $1.2\times10^{-17}$ | Gerakines et al. (1995) |
| $C_2H_6$ | 2976 | $1.1\times10^{-17}$ | Moore & Hudson (1998)[b] |
| | 821 | $1.9\times10^{-18}$ | Pearl et al. (1991) |
| $C_2H_4$ | 1436 | $2.9\times10^{-18}$ | Moore & Hudson (1998)[b] |
| $N_2H_4$ | 2768 | $\sim1.5\times10^{-17}$ | assumed from $NH_3$ |
| $CH_3NH_2$ | 2794 | $\sim5\times10^{-18}$ | assumed from $C_2H_6$ |
| HCN | 2087 | $5.1\times10^{-18}$ | Gerakines et al. (2004) |
| $H_2CO$ | 1500 | $3.9\times10^{-18}$ | Schutte et al. (1993) |
| $CH_3OH$ | 1026 | $2.8\times10^{-17}$ | D'Hendecourt & Allamandola (1986) |
| $CH_3CH_2OH$ | 1044 | $7.3\times10^{-18}$ | Moore & Hudson (1998)[b] |
| $CH_3CHO$ | 1350 | $6.1\times10^{-18}$ | Moore & Hudson (1998)[b] |
| CO | 2139 | $1.1\times10^{-17}$ | Gerakines et al. (1995) |
| $CO_3$ | 2045 | $\sim7.6\times10^{-17}$ | assumed from $CO_2$ |
| $O_3$ | 1045 | $1.4\times10^{-17}$ | Brewer & Wang (1972) |
| $OCN^-$ | 2165 | $1.3\times10^{-16}$ | van Broekhuizen et al. (2005) |

[a] The uncertainties in the tabulated transmission band strengths is ~20–30% when comparing results from different references, ice mixtures and ice temperatures.
[b] In a $H_2O$ ice matrix.

Each abundance is quantified by fitting a local baseline around the spectral feature and then fitting one or multiple Gaussians to the band of interest using a personal IDL routine. The automatic fits are visually inspected to ensure that the fitted Gaussians are consistent with bands in pure and ice mixture reference spectra.

### $CH_4$, $NH_3$ and $CH_4$:$NH_3$ ice photolysis

Figure 1.1 shows the spectra before and after photolysis of pure $CH_4$ ice, pure $NH_3$ ice and a $NH_3$:$CH_4$ ~1:1 ice mixture, all at 20 K. The bands used to quantify the considered photoproducts, $C_2H_6$, $C_2H_4$, $N_2H_4$, $CH_3NH_2$ and HCN, are marked. The strong $C_2H_6$ bands are assigned from spectral comparison alone, since these bands are not confused with any other possible product bands (Moore & Hudson 1998). The $C_2H_4$ band is weaker, but can be assigned by combining spectral comparison with desorption data – the 1436 $cm^{-1}$ feature desorbs with

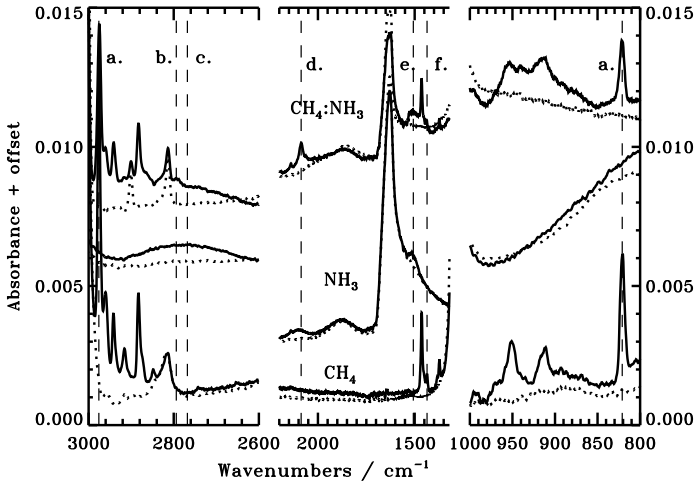


Figure 1.1 The initial (dotted lines) and photolysed spectra (solid lines) of pure $CH_4$ ice, pure $NH_3$ ice and a $NH_3$:$CH_4$ ~3:2 mixture, all at 20 K. The bands used for quantifying the a. $C_2H_6$, b. $CH_3NH_2$, c. $N_2H_4$, d. HCN, e. $NH_2$ and f. $C_2H_4$ ice abundances are marked with dashed lines.

$C_2H_6$ around 60 K in the pure $CH_4$ ice, in agreement with the $C_2H_4$ assignment. The same assignments were made by Gerakines et al. (1996) and Moore & Hudson (1998).

The observed broad band at 2794 $cm^{-1}$ in the pure $NH_3$ ice agrees in band position and width with one of the $N_2H_4$ ice bands reported by (Roux & Wood 1983). The $N_2H_4$ assignment is, however, tentative since no desorption data exist on $N_2H_4$ and most other $N_2H_4$ features overlap with strong $NH_3$ bands. The other probable pure $NH_3$ photoproduct, $N_2H_2$, is excluded as a carrier from comparison with spectra by Blau et al. (1961). Two other bands form in the pure $NH_3$ ice upon UV irradiation, at 2111 and 1507 $cm^{-1}$. The 2111 $cm^{-1}$ is probably due to $N_2H_4$ as well, while the 1507 $cm^{-1}$ band can be assigned to $NH_2$ (Gerakines et al. 1996) though $NH^+_{3/4}$ are candidates as well (Thompson & Jacox 2001). During warm-up most of the band disappears before $NH_3$ desorption, consistent with that $NH_2$ is the main carrier, but with an unconfirmed assignment, its formation cannot be quantified.

The HCN and $CH_3NH_2$ ice features in the photolysed $CH_4$:$NH_3$: ice mixture spectrum are assigned by comparing laboratory ice spectra from the NASA Goddard ice library with spectra from the photolysed $NH_3$:$CH_4$ ice mixture during warm-up. During the TPD experiments following photolysis, mass patterns con-

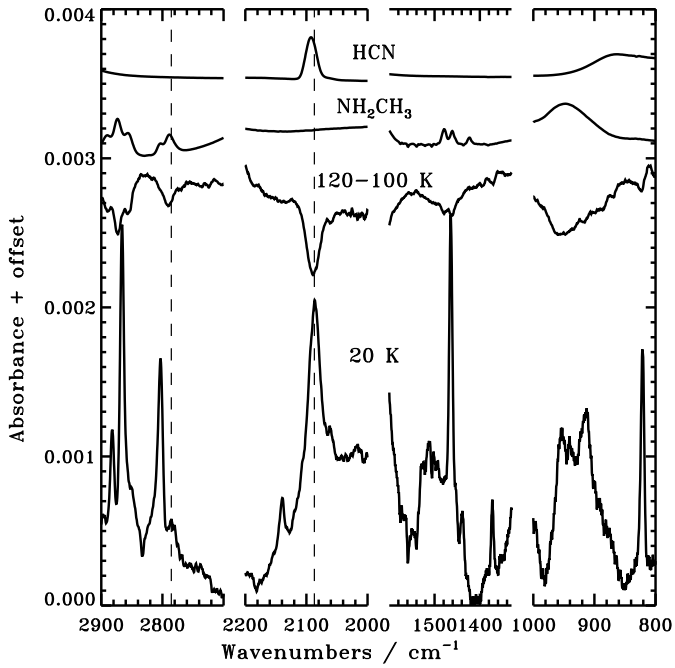


Figure 1.2 Starting from the bottom the figure shows a photolysed $NH_3$:$CH_4$ ice spectrum at 20 K, a difference spectrum during warm-up of the same ice mixture, a $CH_3NH_2$ spectrum (mixed with $H_2O$) and a pure HCN ice spectrum. In the difference spectrum negative peaks signify desorption of the band carrier. The dashed lines show the agreement between the reference spectra and the photolysis experiment for the HCN and $NH_2CH_3$ bands used for quantification.

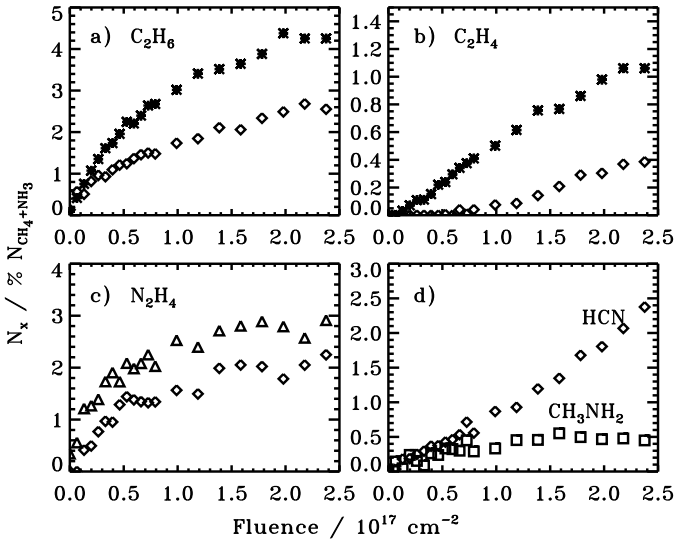


Figure 1.3 The relative formation of five complex molecules, with respect to the initial total ice abundance, in pure $CH_4$ ice (stars), in pure $NH_3$ ice (triangles) and in a $CH_4$:$NH_3$ ~ 3:2 ice mixture (diamonds and squares) as a function of UV fluence at 20 K.

sistent with HCN and $CH_3NH_2$ desorption are visible at 110 and 120 K. Figure 1.2 shows the difference spectrum of the photolysed $NH_3$:$CH_4$ ice mixture between 120 and 100 K, i.e. the spectrum acquired at 100 K subtracted from the spectrum acquired at 120 K. This reveals the spectral features that desorb in this temperature interval. The agreement of this difference spectrum with HCN + $CH_3NH_2$ is excellent. Figure 1.2 also shows that the bands selected to quantify HCN and $CH_3NH_2$ are distinguishable at 20 K.

Quantifying the formation of ice species with respect to the initial ice composition requires known transmission band strengths – all spectra here are acquired with RAIRS, but the relative band strengths are the same in transmission and reflection-absorption mode as long as the bands are not too strong. Transmission band strengths are available for $C_2H_6$, $C_2H_4$ and HCN, but not for $N_2H_2$ or $CH_3NH_2$. The latter two band strengths are estimated by assuming a similar N-H/C-H band strength in the more complex molecules as in $NH_3$ and $C_2H_6$.

Figure 1.3 shows the formation of $C_2H_6$, $C_2H_4$, HCN, $N_2H_2$ and $CH_3NH_2$ as a function of UV fluence in pure $CH_4$ ice, in pure $NH_3$ ice and in the $CH_4$:$NH_3$ ~ 3:2 ice mixture. The $C_2H_6$ and $N_2H_4$ production are only reduced by ~40% each

in the mixtures and this is with respect to the total ice thickness. The production rates of $N_2H_4$ and $C_2H_6$ are thus the same within the uncertainties in the pure $CH_4$ ice and in the ice mixture with respect to the $CH_4$ and $NH_3$ abundances. The abundant $C_2H_6$ formation in the ice mixture indicates that it is mainly the formation of larger hydrocarbons that is suppressed in favor of HCN and $CH_3NH_2$ production in the ice mixture. This is consistent with the reduction in $C_2H_4$ production, which is evidence of that $CH_2$, an ingredient in both $C_2H_4$ and $C_3H_8$ formation, is quickly consumed by reactions with $NH_x$ in the ice mixture.

The two molecules forming from reactions of $NH_3$ and $CH_4$ fragments, $CH_3NH_2$ and HCN, depend differently on UV fluence (Fig. 1.3d.). The $CH_3NH_2$ ice abundances reaches steady-state faster than any other investigated molecule, while the formation rate of HCN increases with fluence, indicative of a HCN formation pathway from first-generation photoproducts, such as $CH_3NH_2$.

By comparing the initial $C_2H_6$ formation in Fig. 1.3a and $C_2H_4$ formation in 1.3b, it is possible to constrain the $CH_4$ photodissociation branching ratio. This is done below using the initial formation cross sections of $C_2H_6$ and $C_2H_4$ in the pure $CH_4$ ice, which are $(3.2 \pm 1.3) \times 10^{-19}$ and $(3.6 \pm 1.5) \times 10^{-20}$ after $4 \times 10^{16}$ photons cm$^{-2}$. Gerakines et al. (1996) finds a comparable $C_2H_6$/$C_2H_4$ product ratio (8/1) following pure $CH_4$ ice photolysis.

The chemistry in the pure and mixed ices are then proposed to proceed as shown in Fig. 1.4, where the reaction scheme for the mixed ice is constructed by combining the $CH_4$ and $NH_3$ reaction schemes with the bridging HCN and $CH_3NH_2$ reactions. The reaction schemes clearly show the additional number of steps required to from HCN compared to $CH_3NH_2$, which explains the initial delay in the HCN production. The early steady-state of $CH_3NH_2$ suggests that it easily photodissociates into HCN and that this is the main formation path of HCN in the ice. This is also consistent the almost constant formation rate of HCN once the initial delay is overcome.

### $CH_4$:$H_2O$ ice mixture photolysis

Figure 1.5 shows the initial and photolyzed spectra of pure $CH_4$ ice and a $H_2O$:$CH_4$ ~1:3 mixture, both at 20 K. There are no identified photoproducts following pure $H_2O$ ice photolysis (not shown). This is in contrast with e.g Gerakines et al. (1996), who detected OH and $H_2O_2$ formation. The observed rates were low, however, and neither would be expected to be observable at the ice thicknesses and UV fluences employed in this study. The photolyzed $CH_4$ and $H_2O$:$CH_4$ ice spectra are plotted together with pure $CH_3OH$, $H_2O$, $CH_3CH_2OH$ and $CH_3CHO$ ice spectra to justify the complex photoproduct assignments. The most isolated

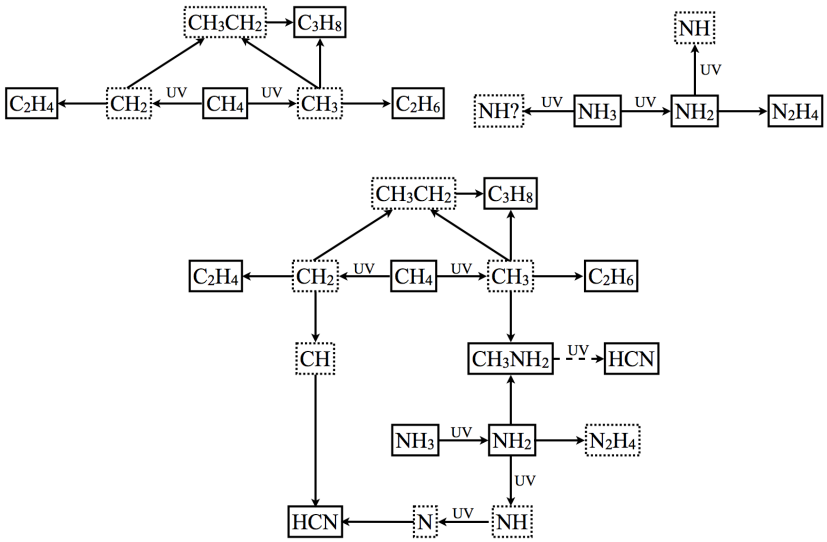


Figure 1.4 The proposed reactions schemes following UV photolysis of pure $CH_4$, pure $NH_3$ ice and a $CH_4$:$NH_3$ ice mixture. Solid boxes mark detected species and dotted boxes undetected ones.

bands of each complex ice species are used for quantification.

Similarly to the $CH_4$:$NH_3$ photochemistry, the formation rate of $C_2H_6$ is almost constant between the pure $CH_4$ ice and the $CH_4$:$H_2O$ 3:1 mixture, while the $C_2H_4$ production is significantly lowered. Of the new complex molecules in the $CH_4$:$H_2O$ mixture, $CH_3OH$ forms the fastest, but reaches a similar steady-state level to $CH_3CH_2OH$. $H_2CO$, $CH_3CHO$ and $CH_3CH_2OH$ all start to form after a certain fluence level is reached, indicative of a second or later generation of photoproducts. $CH_3CHO$ forms last. Qualitatively the product assignments agree with Moore & Hudson (1998) who also found a comparable $CH_3OH$/$CH_3CH_2OH$ product ratio in their $H_2O$:$CH_4$ 2:1 ice mixture.

$CH_3CH_2OH$ and $CH_3CHO$ are also photoproducts of pure $CH_3OH$ ice (Chapter 10) and the product ratio of $CH_3CH_2O$ and $CH_3CHO$ is consistent between the $CH_3OH$ and the $CH_4$:$H_2O$ photolysis experiments. The formation path for $CH_3CH_2OH$ must however be different in the two experiments since the $CH_3CH_2OH$ to $CH_3OH$ ratio is one order of magnitude higher in the $CH_4$:$H_2O$ ice than in the $CH_3OH$ ice following irradiation with the same fluence. Figure 1.7 shows that $CH_3CH_2OH$ probably forms from $C_2H_5$ + OH in the $CH_4$:$H_2O$ mixture versus $CH_3$+$CH_2OH$ in the $CH_3OH$ ice (Chapter 10), while $CH_3CHO$ forms through

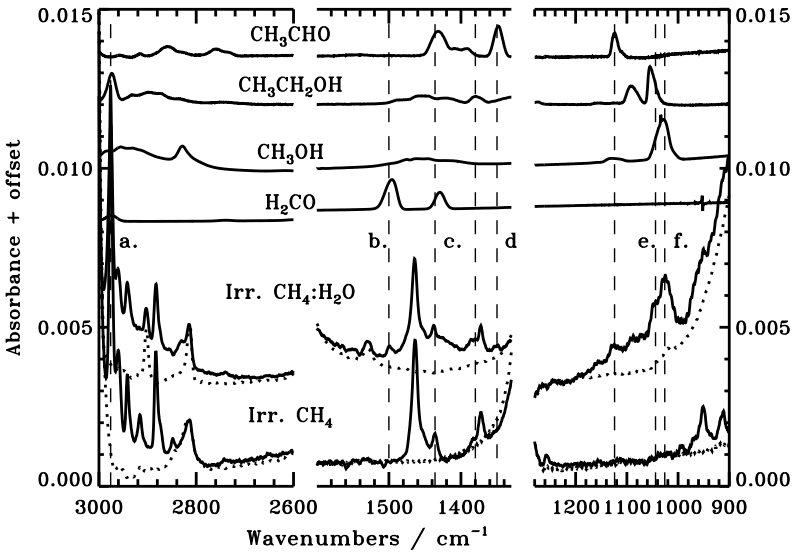


Figure 1.5 The initial (dotted lines) and photolysed spectra (solid lines) of pure $CH_4$ ice and a $CH_4$:$H_2O$~3:1 mixture, both at 20 K. The bands used for quantifying the a. $C_2H_6$, b. $H_2CO$, c. $C_2H_4$, d. $CH_3CHO$, e. $CH_3CH_2OH$ and f. $CH_3OH$ ice abundances are marked with dashed lines.

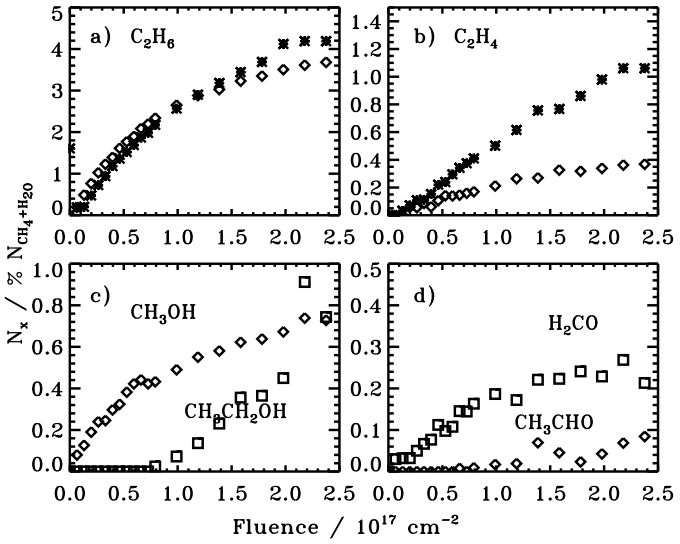


Figure 1.6 The relative formation of six complex molecules, with respect to the initial total ice abundance, in pure $CH_4$ ice (stars) and in a $H_2O$:$CH_4$ ~1:3 ice mixture (diamonds and squares) as a function of UV fluence at 20 K.

photodissociation of $CH_3CH_2OH$ or possibly radical-radical reactions between $CH_3$ and HCO in both cases; both formation paths are consistent with the late onset of $CH_3CHO$ formation. The delay in $H_2CO$ and $CH_3CH_2OH$ formation is also explained by the reaction scheme, which shows that both species requires one more reaction step compared to $CH_3OH$ and $C_2H_6$ formation.

### Pure $CO_2$ and $CH_4$:$CO_2$ ice photolysis

Pure $CO_2$ ice photolysis results in CO, $CO_3$ and $O_3$ formation, consistent with Gerakines et al. (1996) Figure 1.8 shows that in the $CH_4$:$CO_2$ ice mixture CO and $CO_3$ still forms and so does $C_2H_6$ ad $C_2H_4$. In addition, features belonging to $CH_3OH$, $H_2CO$ and $CH_3CHO$ are identified. HCOOH probably forms as well, but its most distinct bands overlaps with features from $H_2CO$, $CH_3CHO$ and $CH_3COOH$. The contribution of HCOOH to the 1700 $cm^{-1}$ complex can be investigated through difference spectra during warm-up, since the HCOOH desorption temperature is known from Chapter 10. This is shown in Fig. 1.9, where a HCO-X band disappears in the 130–160 K temperature range, where HCOOH desorbs. It is however not possible to determine the HCOOH formation during irradiation.

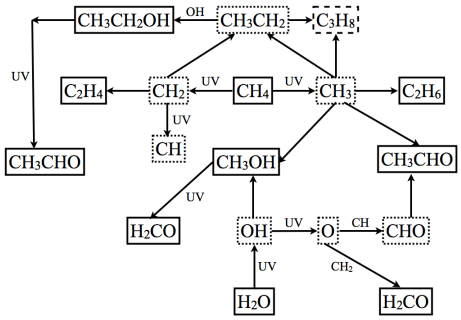


Figure 1.7 The proposed reactions scheme following UV photolysis of a $CH_4$:$H_2O$ ice mixture. Solid boxes mark detected species, dashed boxes tentatively detected species from RAIRS or TPD curves and dotted boxes undetected species.

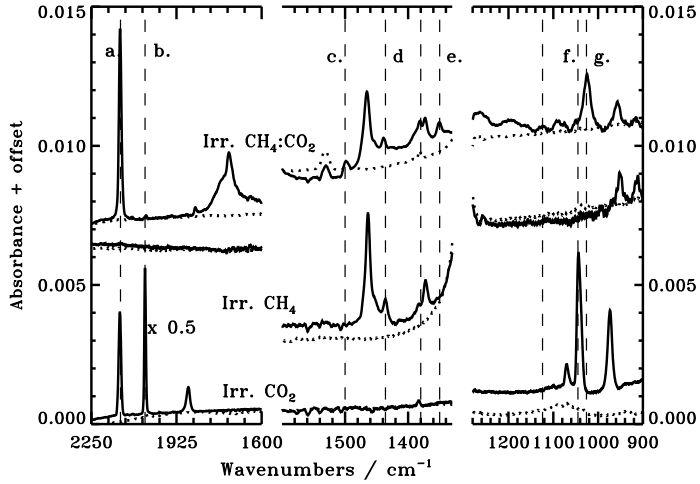


Figure 1.8 The initial (dotted lines) and photolysed spectra (solid lines) of pure $CO_2$ ice, pure $CH_4$ ice and a $CO_2$:$CH_4$ ~1:2 mixture, all at 20 K. The bands used for quantifying the a. CO, b. $CO_3$, c. $H_2CO$, d. $C_2H_4$, e. $CH_3CHO$, f. $O_3$ and g. $CH_3OH$ ice abundances are marked with dashed lines.

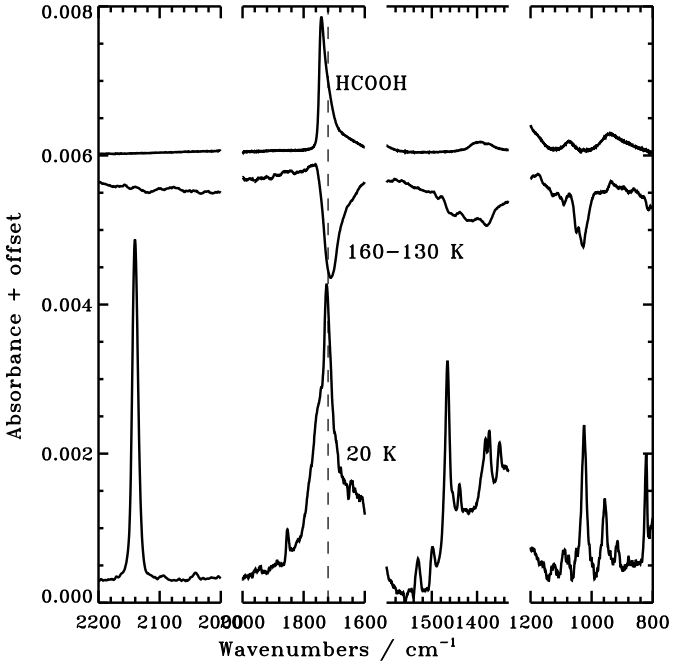


Figure 1.9 Starting from the bottom the figure shows a photolysed $CO_2$:$CH_4$ ice spectrum at 20 K, a difference spectrum during warm-up of the same ice mixture, and a pure HCOOH spectrum. In the difference spectrum negative peaks signify desorption of the band carrier.

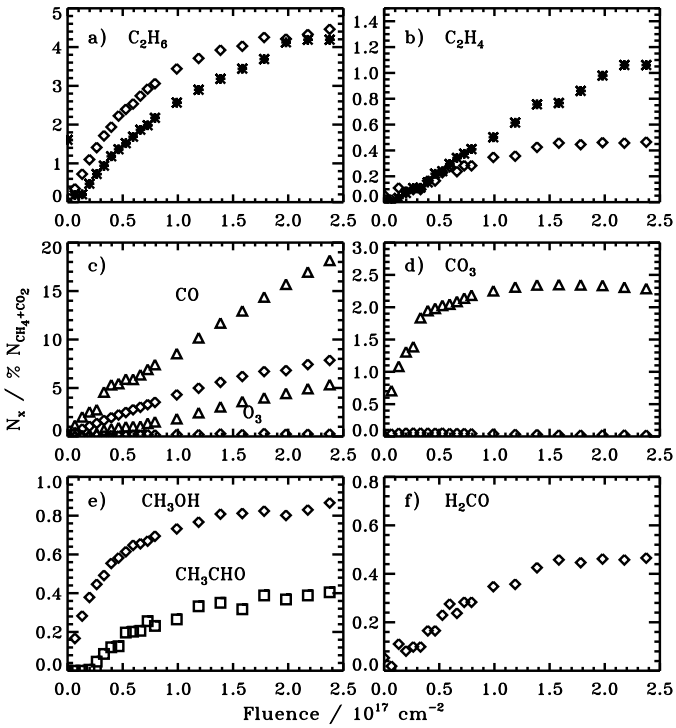


Figure 1.10 The relative formation of eight photoproducts, with respect to the initial total ice abundance, in pure $CH_4$ ice (stars), pure $CO_2$ ice (triangles) and a $CH_4$:$CO_2$ ~ 2:1 ice mixture (diamonds and squares) as a function of UV fluence at 20 K.

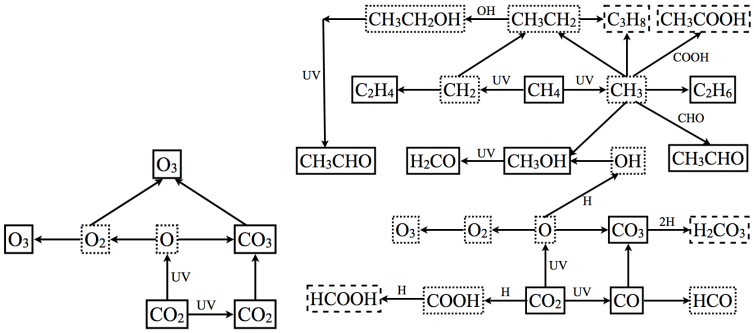


Figure 1.11 The proposed reactions schemes following UV photolysis of pure $CO_2$ ice and a $CH_4$:$CO_2$ ice mixture. Solid boxes mark detected species, dashed boxes tentatively detected species and dotted boxes undetected ones.

Therefore the quantitative analysis focuses on the other, securely identified ice photoproducts. $CO_3$ and $O_3$ formation changes most dramatically between pure $CO_2$ photolysis and $CH_4$:$CO_2$ photolysis; the formation rates decrease with an order of magnitude in the mixture (Fig. 1.10). The CO formation rate does not change significantly indicating that CO is relatively unreactive. The $C_2H_6$ formation rate is enhanced in the mixture compared to the pure ice. Of the three new complex species, $CH_3OH$ is formed most abundantly – hydrogenation of O atoms must be very efficient. $CH_3CHO$ and $H_2CO$ form as well and in higher abundances compared to the $H_2O$:$CH_4$ mixture.

The extremely low $CO_3$ production in this ice mixture can be explained by fast hydrogenation of $CO_3$ to form $H_2CO_3$. Moore (1991) detected abundant $H_2CO_3$ during warm-up of an irradiation $H_2O$:$CO_2$ ice mixture and similar bands are also present during warm-up of the $CH_4$:$CO_2$ ices to 200 K.

Figure 1.11 shows this reaction path and proposed reaction paths for all infrared-detected products. Th faster onset of $CH_3CHO$ production in the $CH_4$:$CO_2$ ice mixture compared to the $H_2O$:$CH_4$ ice mixtures suggests that $CH_3$ + HCO is the dominating formation path in the $CH_2O$:$CH_4$ ice rather than $CH_3CH_2OH$ photodissoication. HCOOH formation may occur through two different reaction pathways: hydrogenation of $CO_2$ and CO+HCO reactions. The former is prohibitively slow for thermalized hydrogen atoms (Bisschop et al. 2007a), but it may still be fast for energetic species. In either case, the experiments here shows that any kind of hydrogenation of CO and $CO_2$ is definitely less efficient than hydrogenation of the radical $CO_3$. This is in agreement with previous comparison of molecule and

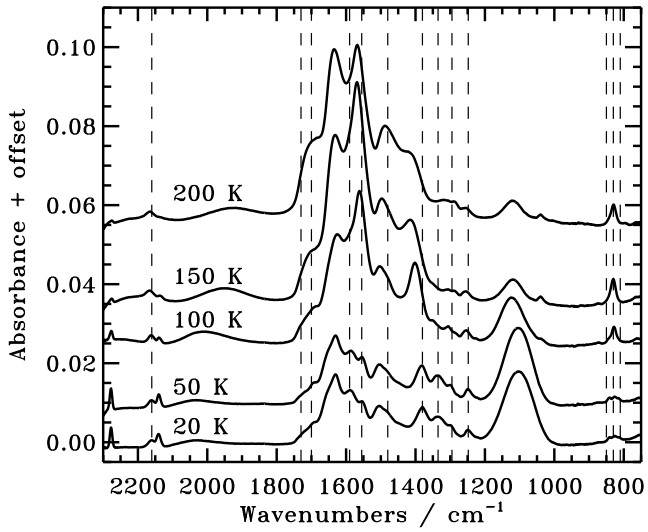


Figure 1.12 spectrum of irradiated $NH_3$:$CO_2$ ice during warm-up. All features exclusive to photolysis of $CO_2$:$NH_3$ ice mixtures compared to pure ices are marked with dashed lines. The $OCN^-$ feature is at 2161 $cm^{-1}$.

atom hydrogenation efficiencies (Hiraoka et al. 1998).

### $CO_2$:$NH_3$ ice mixture photolysis

Irradiation of a $CO_2$:$NH_3$ ice mixture produces a complex ice spectrum (Fig. 1.12). This has been previously noted for ice mixtures containing $NH_3$, $H_2O$ and CO and many of the new broad features can be ascribed to $NH_4^+$ salts and $XCOO^-$ ions (Muñoz Caro & Schutte 2003). Considering the simple mixture, most of $XCOO^-$ should be $HCOO^-$ and $HCOOO^-$, but some more complex products cannot be excluded. Another probable product is $NH_2CHO$, which has several spectral features in the 1400-1700 $cm^{-1}$ region. Because of the overlap between different bands shown in Fig. 1.12, only the formation of CO and $OCN^-$ (from its 2161 $cm^{-1}$ band) can be quantified at this stage.

$OCN^-$ is a common product from UV processing of C, O and $NH_3$ containing ices and its formation in the $NH_3$:$CO_2$ ice mixture is consistent with previous studies (e.g. van Broekhuizen et al. 2004). Figure 1.13 shows that similarly to what was observed for HCN in the $NH_3$:$CH_4$ mixture, $OCN^-$ is not produced immediately at the onset of irradiation, indicative of a multi-step formation process.

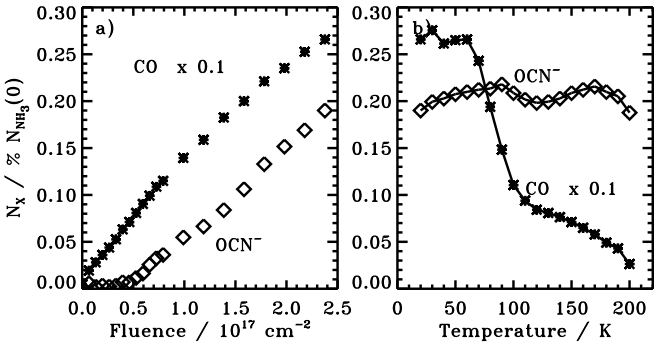


Figure 1.13 The evolution of the $OCN^-$ and CO abundances as a function of UV fluence during irradiation, and as a function of temperature during warm-up.

This explains the low yield of $OCN^-$ with respect to $NH_4^+$; the lower limit on $NH_4^+$ formation is more than an order of magnitude greater than the $OCN^-$ production. $OCN^-$ is thus not the main counter ion of $NH_4^+$. Figure 1.13 also shows that $OCN^-$ does not desorb below 170 K.

With only two band assignments the $CO_2$:$NH_3$ reaction scheme is speculative. The pathway to HNCO and further to $OCN^-$ may either be through CO+NH or CO+$NH_2$ followed by photodissociation. From the $H_2O$:$CO_2$ and $CH_4$:$CO_2$ ice mixtures, both $H_2CO_3$ and HCOOH are expected products in the $CO_2$:$NH_3$ ice photolysis experiment. These two acids may very well be the main counter ions to $NH_4^+$, since in the presence of $NH_3$ they should both be converted into their salt counter parts (Schutte & Khanna 2003).

### The effect of $H_2O$ at different concentrations

Figure 1.14 shows the spectra of pure $NH_3$, $H_2O$:$NH_3$ 1:1 and $H_2O$:$NH_3$ 4:1 ice before and after the ices are irradiated with a UV fluence of $2.3 \times 10^{17}$ cm$^{-2}$. Adding different amounts of $H_2O$ to the $NH_3$ ices suppresses the production of the 2111 cm$^{-1}$ and 2768 cm$^{-1}$ features, observed in the pure ice photolysis experiment and there ascribed to $N_2H_4$; neither is observed in any of the $H_2O$:$NH_3$ ice mixture experiments, though overlap between the 2768 cm$^{-1}$ band and the $H_2O$ feature wing prevents a strict upper limit. The 1507 cm$^{-1}$ band is observed in the $H_2O$ mixtures. In addition, at least one new feature appears in the 4:1 ice mixture, and probably in the 1:1 ice as well, at 1470 cm$^{-1}$. The 1470 and 1507 cm$^{-1}$ bands are fitted simultaneously with two Gaussians to take into account the band

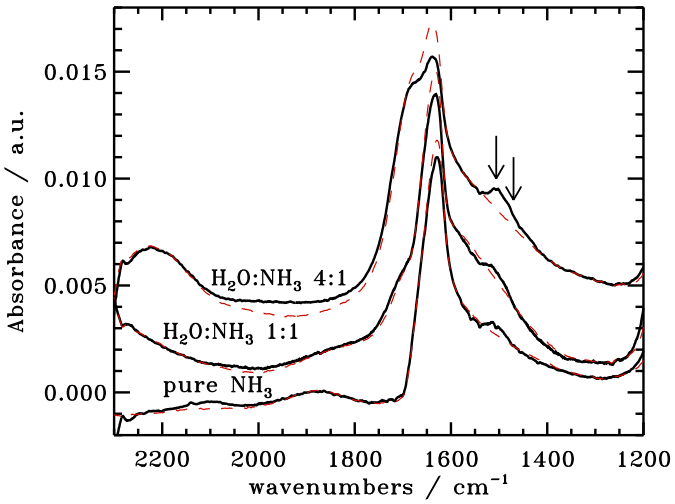


Figure 1.14 Spectra of pure $NH_3$ ice, $NH_3$:$H_2O$ 1:1 and 1:4 ice mixtures, before irradiation at 20 K (dashed lines) and after irradiation at 20 K (solid lines). The changing 1507 and 1470 $cm^{-1}$ features are marked with arrows.

overlaps. In general the combined band around 1500 $cm^{-1}$ is more pronounced the more $H_2O$ is added, indicative of either the onset of an acid-base chemistry or efficient trapping of $NH_2$. Only additional irradiation experiments will be able to distinguish between the two carrier scenarios. Without a more strict assignment, the chemistry cannot be further quantified in the $H_2O$:$NH_3$ mixtures.

Photolysis of the $H_2O$:$CO_2$ mixtures result in several broad features, which are due to a combination of HCOOH and $H_2CO_3$. The bands cannot be easily separated during irradiation and therefore this chemistry is difficult to quantify as well.

In the $CH_4$:$H_2O$ 3:1 and 1:2 ice mixtures $C_2H_6$, $CH_3OH$, $CH_3CHO$, $H_2CO$ and $CH_3CH_2OH$ all clearly form upon UV irradiation. The formation of the first four complex species are quantified in Fig. 1.15 with respect to the initial $CH_4$ ice abundance. Increasing the $H_2O$ concentration reduces the relative $C_2H_6$ formation and increases the relative formation rates of $CH_3OH$, $CH_3CHO$ and $H_2CO$ as expected when increasing the relative OH/$CH_3$ radical ratio in the ice.

During irradiation there is no obvious evidence for a slower radical diffusion because of higher binding energies in a $H_2O$-rich ice. During warm-up there are some differences between the two ice mixtures, however (Fig. 1.16). The $CH_3OH$ and $CH_3CHO$ abundances increase in both mixtures with temperature, but the $CH_3CHO$ abundances increases more in $H_2O$-rich ice and $CH_3OH$ in the $H_2O$-poor ice, indicative of different diffusion conditions in the $H_2O$-poor and the more strongly bound $H_2O$-rich mixture.

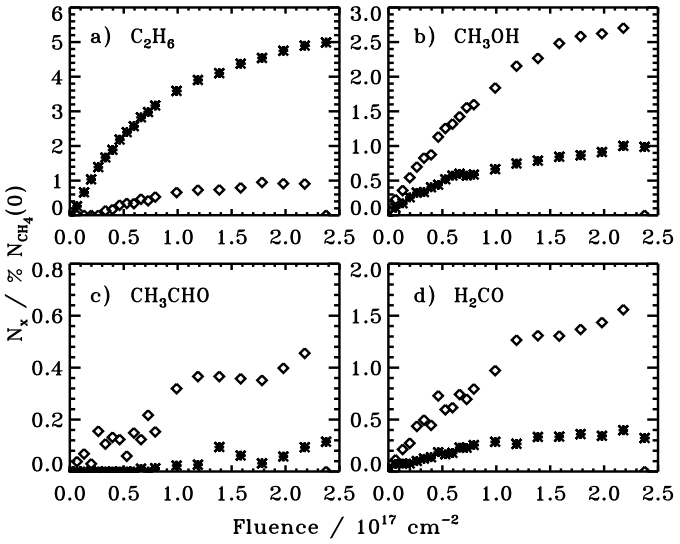


Figure 1.15 The relative formation of four complex molecules in $CH_4$:$H_2O$~3:1 and 1:2 ice mixtures (stars and diamonds, respectively) with respect to the initial $CH_4$ ice abundance as a function of UV fluence at 20 K.

### $NH_3$ ice photodesorption

The photochemistry in both pure ices and mixtures is limited by the formation rates of radicals through photodissociation, which is discussed in the next subsection, and by the photodesorption rate, which continuously desorbs ice. Figure 1.17 shows the loss of $NH_3$ ice at 20 K as a function of UV fluence due to a combination of bulk dissociation and surface photodesorption, calculated from the 1070 cm$^{-1}$ band. The photodesorption yield is determined from the linear decrease in ice thickness, visible at later times, while the bulk dissociation follows an exponential decay (Öberg et al. 2009b,a). The combined linear and exponential fits result in a $NH_3$ photodesorption yield of $(1.2 \pm 0.7) \times 10^{-3}$ per incident UV photon. The main error comes from the ice thickness uncertainty; the fit error is ~15%.

The derived photodesorption yield is similar, within a factor of three, to the yields determined previously for CO, $CO_2$, $H_2O$ and $CH_3OH$ (Öberg et al. 2009a,b, Chapter 10), confirming the assumption of an almost constant photodesorption yield for all ices with strong UV absorptions (Chapter 12).

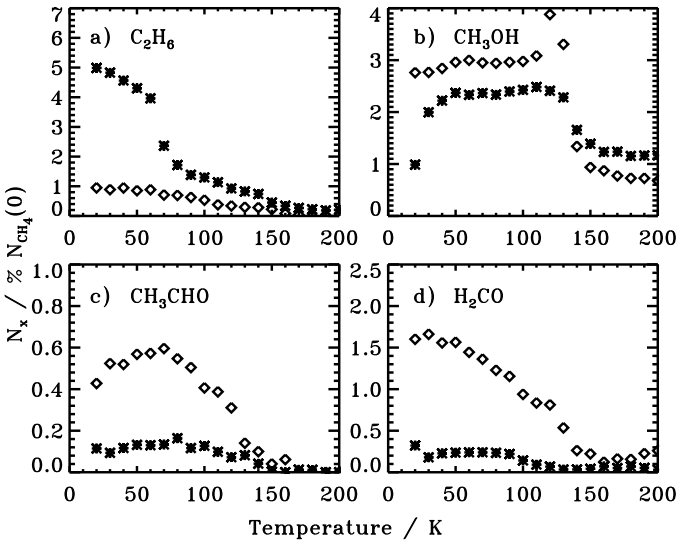


Figure 1.16 The relative evolution of four complex molecules in $CH_4$:$H_2O$~3:1 and 1:2 ice mixtures (stars and diamonds, respectively) as a function of temperature during warm-up.

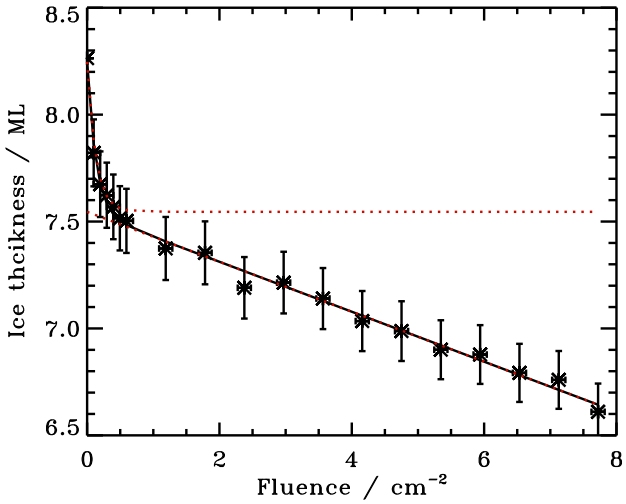


Figure 1.17 The loss in $NH_3$ (stars) ice due to bulk dissociation (exponential part) and surface photodesorption (linear part). The combined fit is plotted with a solid line and the linear and exponential parts are overplotted with dotted lines.

**$NH_3$ and $CH_4$ photodestruction**

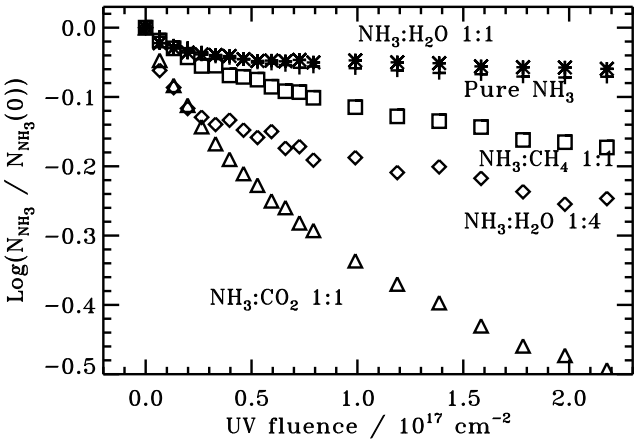


Figure 1.18 The log-transformed normalized photodestruction rate of pure $NH_3$ ice (stars), $NH_3$:$H_2O$ 1:1 (crosses), $NH_3$:$CH_4$ 2:3 (squares), $NH_3$:$CO_2$ 2.5:1 (triangles) and $NH_3$:$H_2O$ 1:4 (diamonds).

Figure 1.18 shows the normalized and log-transformed loss of $NH_3$ ice as a function of fluence for different ice mixtures. In contrast to Fig. 1.17 the ices are thick (~50 ML) and the fluence scale short to ensure that bulk processes dominate the ice loss, rather than photodesorption of surface molecules. The measured photodestruction rates for $NH_3$ during the first $4 \times 10^{16}$ photons cm$^{-2}$ are reported in Table 1.1 for pure $NH_3$, ~$NH_3$:$H_2O$/$CH_4$/$CO_2$ 1:1–3 mixtures and a $NH_3$:$H_2O$ 1:4 mixture.

The photodissociation rate for pure $NH_3$ ice is $1.0 \times 10^{-18}$ cm$^{-2}$. This is an order of magnitude lower than the measured gas phase photodesorption cross section (van Dishoeck 1988). A similar discrepancy was previously found for $CH_3OH$, indicative of that fast recombination is important following ice photodissociation. The new $NH_3$ ice photodissociation rate is however a factor of 8 higher than previously measured for a thick $NH_3$:$N_2$ 1:10 ice mixture, which is probably the most comparable measurement to the present one, since all previous photodissociation measurements are for thick ices and thick pure ices (of 1000 ML or more) suffer from optical depth effects (Cottin et al. 2003). Furthermore Cottin et al. (2003) measured the photodissociation yield for an order of magnitude higher fluence, when back reactions become important – if the destruction cross section is measured over $2.3 \times 10^{17}$ photons cm$^{-2}$ it would appear to be the same as measured by Cottin et al. (2003) for the 1:10 ice within the experimental uncertainties. The higher photodissociation yield measured here should thus be more accurate, even though the precision of the measurements by Cottin et al. (2003) was higher.

The initial $NH_3$ photodestruction rate is indistinguishable in the $NH_3$:$H_2O$ 1:1 mixtures, the $NH_3$:$CH_4$ 2:3 mixtures and the pure $NH_3$ ice. At higher fluences there is still no measurable difference between the $NH_3$ photodissociation in pure $NH_3$ ice and in the $NH_3$:$H_2O$ mixture, while more $NH_3$ is being destroyed in the $NH_3$:$CH_4$ ice mixture. This difference suggests an efficient chemistry in the $NH_3$:$CH_4$ ice, which slows down the reformation of $NH_3$ from photodissociation fragments.

The initial photodestruction is significantly higher in the $NH_3$:$CO_2$ 2.5:1 and the $NH_3$:$H_2O$ 1:4 ice mixtures compared to pure $NH_3$ ice (the quoted uncertainties in Table 1.1 include the systematic uncertainties, the fit uncertainties are $\sim 0.2\times10^{-18}$ cm$^2$). In addition the destruction rate in the $NH_3$:$CO_2$ ice does not slow down with UV fluence. The higher initial photodestruction rate suggests an additional destruction mechanism than photodissociation such as UV induced acid-base chemistry i.e. $NH_3$ is both destroyed directly by the UV irradiation through photodissociation and indirectly through protonation in reactions with other photoproducts. This is the only explanation for the high destruction rate in the $NH_3$:$CO_2$ ice mixture. The high rate in the 4:1 $H_2O$:$NH_3$ ice may also be due to a slower diffusion rate in a $H_2O$-rich ice, which limits back reactions. Both alternatives are discussed below together with new experiments that will constrain the relative importance of the two mechanisms.

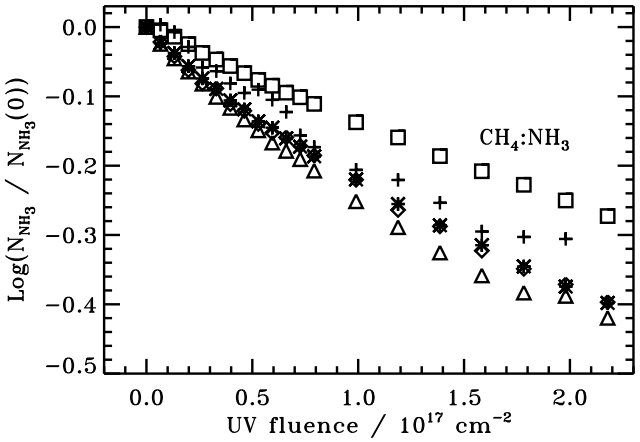


Figure 1.19 The log-transformed normalized photodestruction rate of pure $CH_4$ ice (stars), $CH_4$:$H_2O$ 3:1 (crosses), $CH_4$:$NH_3$ 3:2 (squares), $CH_4$:$CO_2$ 2:1 (triangles) and $CH_4$:$H_2O$ 1:2 (diamonds).

None of this behavior is observed for $CH_4$ photodestruction in a similar set of ice mixtures (Fig. 1.19). Except for a 50% lower photodestruction cross-section in the $CH_4$:$NH_3$ mixture, all $CH_4$ cross-sections are $\sim 2.5\times10^{-18}$ cm$^2$, which is a factor of three higher than previously reported by Gerakines et al. (1996) and

a factor of five lower than the gas phase value (van Dishoeck 1988). The factor of two smaller discrepancy between ice and gas phase $CH_4$ compared to the $NH_3$ case, is consistent with the expected higher volatility of $CH_{2/3}$ than $NH_2$; the faster diffusion of $CH_{2/3}$ should reduce the importance of immediate back reactions.

### 1.3.2 Testing complex ice formation in an astrophysical ice equivalent

The comparison between photolysis of pure and binary mixtures shows that the binary reactions products are consistent with combining the pure reaction schemes with a few bridging reactions. In tertiary ice mixtures and in a four-component astrophysical ice analogue, the products are therefore expected to be consistent with the products from the binary mixtures, with some new bridging reactions combining e.g. the $CH_3NH_2$ and HCOOH products to form $NH_2CH_2COOH$ in a $NH_3$:$CH_4$:$CO_2$ ice.

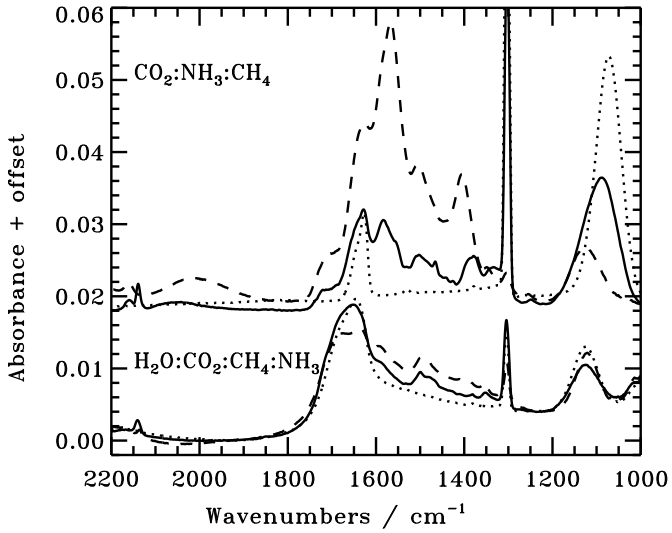


Figure 1.20 Infrared spectra of an astrophysical ice equivalent and the $NH_3$:$CO_2$:$CH_4$ ice mixture before irradiation at 20 K (dotted line), following photolysis at 20 K (solid line) and after warm-up to 100 K (dashed line).

The RAIR spectra following photolysis of these ice mixtures are complicated and few of the products can be quantified spectroscopically (Fig. 1.20. Some attempts to assign peaks around 1500-1700 $cm^{-1}$ have been made in previous studies following photolysis of comparable ice mixtures (Muñoz Caro & Schutte 2003), but this is not pursued here. Instead the carriers of bands outside of the 1500-1700 $cm^{-1}$ spectral region, which can be securely assigned, are quantified

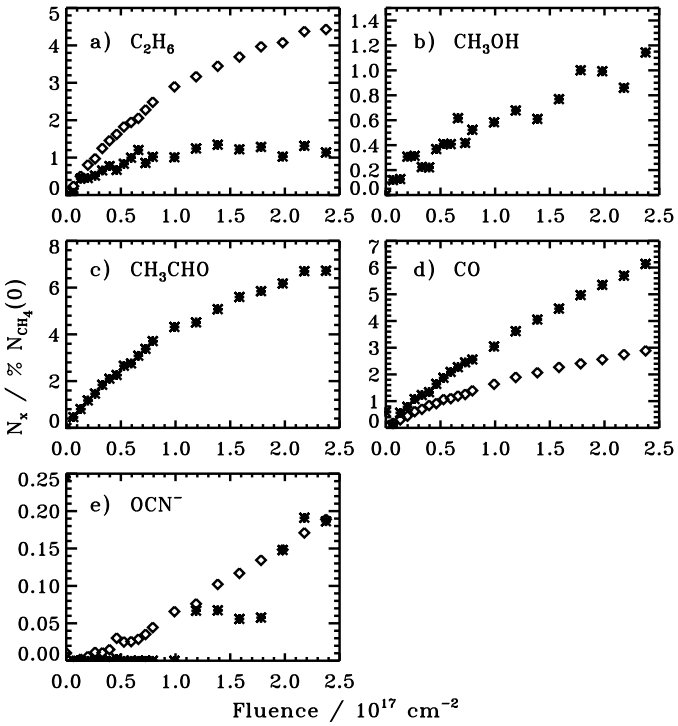


Figure 1.21 The relative evolution of five photoproducts with respect to the initial $CH_4$ ice abundance in a $H_2O$:$CO_2$:$NH_3$:$CH_4$ 100:20:8:12 astrophysical ice equivalent (stars) and three molecules in a $CO_2$:$NH_3$:$CH_4$ ice mixture (diamonds) as a function of fluence at 20 K.

using RAIRS. More complex products are then investigated through TPD experiments. No experiments resulted in any remaining residue after heating to room temperature as have been observed in some previous experiments on thicker ices and after higher UV fluences (Greenberg 1983; Schutte & Khanna 2003).

**Quantification of photolysis through RAIRS**

Despite the complexity of the spectra $C_2H_6$, $CH_3OH$, CO and $OCN^-$ formation can be identified in the astrophysical ice equivalent ( $H_2O$:$CO_2$:$NH_3$:$CH_4$ 100:20:8:12) and in a tertiary $CO_2$:$NH_3$:$CH_4$ 1:1:1 ice mixture, through the same spectral features as in the binary ice mixtures. $CH_3CHO$ probably forms as well though there are alternative nitrogen-bearing carriers of the 1350 $cm^{-1}$ band. A

comparable amount of $OCN^-$ forms in both ice mixtures with respect to the $CH_4$ content in the ice, but the initial formation rate is lower in the $H_2O$-rich ice. The $C_2H_6$ formation is significantly reduced in the $H_2O$-rich ice compared to the tertiary ice mixture, suggesting that most of the $CH_3$ radicals react with other radicals than $CH_3$ in the $H_2O$-rich matrix forming some of the observed $CH_3OH$ and possibly $CH_3CHO$. Overall, the photochemistry in the astrophysical ice equivalent is qualitatively comparable to the simpler ice mixtures.

Table 1.3 lists the formation cross sections for all detected photoproducts with known band strengths in the quantified experiments. These cross sections have a physical meaning for species that form directly through photodissociation, such as CO. For the other molecules it is simply a convenient measure of the initial photoproduction rate – the cross sections are calculated by fitting a line to the growth curves during the first $4 \times 10^{16}$ photons $cm^{-2}$. This growth regime is linear and should only be marginally affected by back-reactions, except for the fast initial recombination reactions immediately following photodissociation. The cross sections are listed with respect to initial $CH_4$, $NH_3$ and $CO_2$ abundances where relevant, i.e. where the product can form from photodissociation fragments of the molecule. The $C_2H_6$ formation is thus only listed with respect to the initial $CH_4$ abundance, while the $CH_3NH_2$ formation is listed with respect to both the $CH_4$ and $NH_3$ abundance.

Table 1.3 Cross sections with respect to the initial $CH_4$/$NH_3$/$CO_2$ abundances.

| Experiment | Photoproduction cross-sections / $10^{-19}$ $cm^2$ | | | | | | |
|---|---|---|---|---|---|---|---|
| | $C_2H_6$ | $C_2H_4$ | $CH_3OH$ | $CH_3CHO$ | CO | $CO_3$ | $OCN^-$ |
| Pure $CH_4$ | 3.2 | 0.36 | | | | | |
| Pure $CO_2$ | | | | | 13 | 5.5 | |
| $CH_4$:$NH_3$ | 4.2 | 0 | | | | | |
| $CH_4$:$CO_2$ | 7.7 | 0.6 | 2.4/–/4.3 | 0.34/–/0.62 | 14 | 0 | –/–/0.5 |
| $CH_4$:$H_2O$ 3:1 | 5.0 | 0.30 | 1.1/–/– | 0.27/–/– | | | |
| $CH_4$:$H_2O$ 1:2 | 2.8 | <0.92 | 10/–/– | 1.9/–/– | | | |
| $CH_4$:$NH_3$:$CO_2$ | 3.8 | | | | 2.2 | | –/0.03/0.03 |
| Astro mix | 2.0 | | 0.83/–/0.33 | 3.7/–/1.5 | 1.5 | | –/0/0 |

The initial formation rate of $C_2H_6$ is constant between the different experiments within a factor of three of the pure ice experiment. In contrast the $C_2H_4$ rate is below the detection limit of $\sim 10^{-20}$ $cm^2$ in the $CH_4$:$NH_3$ mixture and the rate thus changes by an order of magnitude. In most cases the final abundance of these two molecules depend on the steady-state between formation and destruc-

tion in the different ices, rather than the initial formation rate; e.g. the final $C_2H_6$ abundance in the analogue is 1% with respect to $CH_4$ and 4% in the pure $CH_4$ ice, but the initial rate is less than 50% different.

The $CH_3OH$ formation rate varies by an order of magnitude with respect to the initial $CH_4$ and $CO_2$ abundances in the different mixtures, indicating that the formation rate is dominated by the availability of OH radicals in the ice under most conditions, rather than the availability of $CH_3$. It is however also reduced in the analogue where $H_2O$ ice is abundant; $H_2O$ may be too abundant in this case, caging any formed $CH_3$ and OH radicals from diffusing through the ice.

The CO production with respect to the $CO_2$ content is not affected by the presence of $CH_4$ and $NH_3$. It is however reduced by an order of magnitude in the $NH_3$-containing ices where acid base chemistry is feasible, i.e. the tertiary ice mixture and the analogue. In contrast the $CO_3$ formation rate is reduced by an order of magnitude between the pure $CO_2$ ice and all other ice mixtures.

There are thus some significant quantitative differences between the binary ices and the astrophysical ice mixture analogue, which are difficult to predict without a quantitative model that takes into account the effects of acid-base chemistry and different diffusion barriers in different ices.

Nevertheless, the fact that the expected photoproducts are formed in the tertiary ice and the analogue suggest that the initial hypothesis on the reactions schemes for these ices is correct; i.e. the chemistry consist of the binary ice reactions together with bridging reactions resulting in the formation of more complex molecules. Larger molecules should thus be present in the the tertiary and analogue mixtures. This is the topic of the next section.

### TPD experiments

This section investigates the TPD curves of the photolysed astrophysical ice equivalent $H_2O$:$CO_2$:$NH_3$:$CH_4$ 100:20:12:8, together with TPD curves of five other photolyzed ice mixtures. The aim is to constrain which complex molecules form abundantly in the astrophysical ice equivalent by investigating the mass signals at each desorption peak and similarities and differences between the different experiments.

The ices employed for comparison are the $NH_3$:$CO_2$ 1:1, $NH_3$:$CH_4$ 1:1, $NH_3$:$CO_2$:$CH_4$ 1:1:1, $NH_3$:$CO_2$:$H_2O$ 1:1:1 and $H_2O$:$CO_2$:$CH_4$ 1:1:1 mixtures. All mixtures contain similar amounts of $NH_3$, $CH_4$ and $CO_2$ ice initially, within a factor of two, expect for the analogue. All TPD curves are scaled by the same factor and the resulting TPD curves should thus reflect the different formation efficiencies of different products in different ice mixtures.

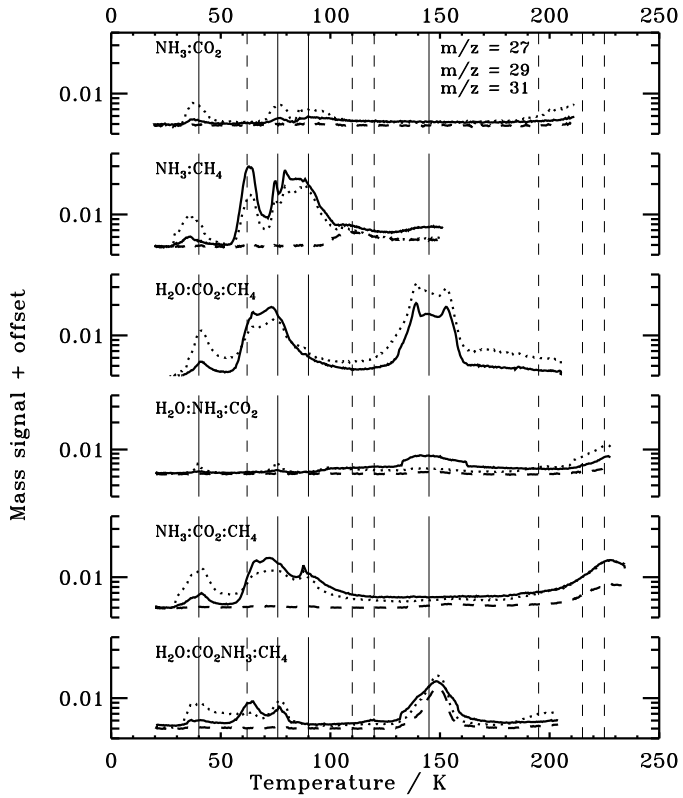


Figure 1.22 TPD curves following photolysis of six ice mixtures for $m/z$=27 (solid), 29 (dotted) and 31 (dashed). The thin solid lines mark the approximate desorption temperatures of $CH_4$, $CO_2$, $NH_3$ and $H_2O$. The thin dashed lines mark the desorption temperatures of different photolysis products, visible in at least one of the TPD experiments.

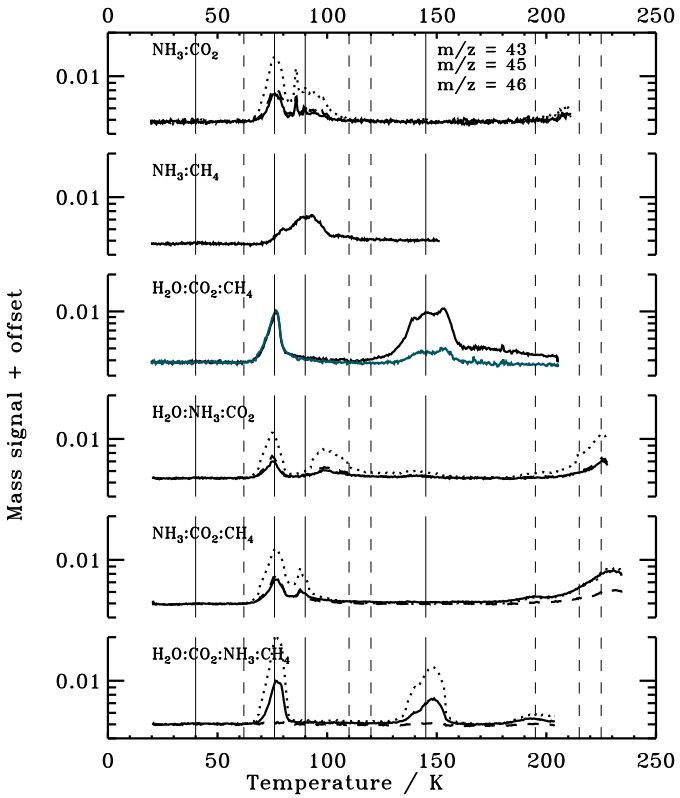


Figure 1.23 TPD curves following photolysis of six ice mixtures for $m/z$=43 (solid), 45 (dotted) and 46 (dashed). The thin solid lines mark the approximate desorption temperatures of $CH_4$, $CO_2$, $NH_3$ and $H_2O$. The thin dashed lines mark the desorption temperatures of different photolysis products, visible in at least one of the TPD experiments.

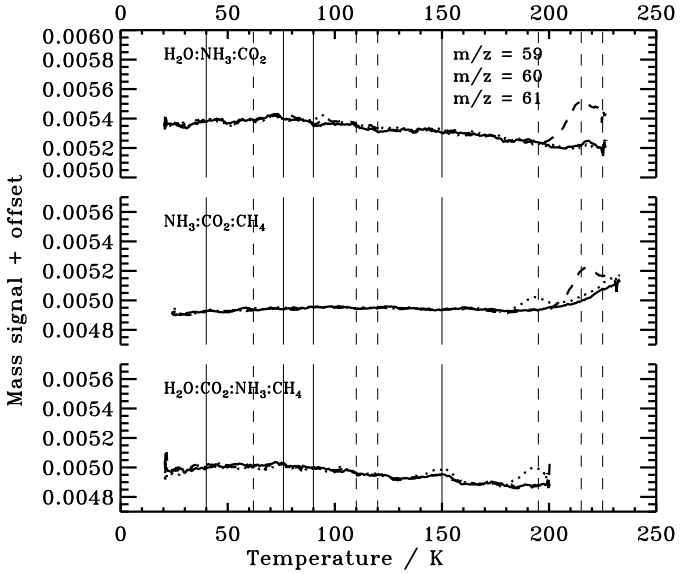


Figure 1.24 TPD curves following photolysis of six ice mixtures for $m/z$=59 (solid), 60 (dotted) and 61 (dashed). The thin solid lines mark the approximate desorption temperatures of $CH_4$, $CO_2$, $NH_3$ and $H_2O$. The dashed lines mark the desorption temperatures of different photolysis products, visible in at least one of the TPD experiments.

Figures 1.22–1.24 present TPD curves for the nine $m/z$ signals, which together contain all desorption peaks observed in the entire set of experiments. The nine $m/z$ are 27, 29, 31, 41, 43, 45, 59, 60 and 61, which trace $C_2H_{4/6}$ (27, 29), HCN (27), $CH_3NH_2$ (27, 29, 31), $H_2CO$ (29), $CH_3OH$ (29, 31), $NH_2OH$ (31), $CH_3CN$ (41), HNCO (43, 27), HCOOH (29, 45), $CH_3COOH$ (45, 60), $NH_2COOH$ (45, 61), $NH_2CH_2COOH$ (29, 45, 59), $CH_3NH_2COOH$ (29, 45, 60), $H_2CO_3$ (45, 61). $m/z$ with contributions from the original ice components are purposefully avoided, i.e. $m/z$=12–18, 28 and 44, since desorption of the original ice components tend to dominate these mass signals.

The ices are at most heated to 230 K, because of experimental constraints, at which point ices are still desorbing. The desorption peaks are analysed sequentially starting with this desorption feature around 230 K and then proceeding to lower temperatures. The resulting assignments to the desorption peaks are summarized in Table 1.4.

The 230 K desorption peak in Figs. 1.22–1.24 is present in the $NH_3$:$CO_2$:$CH_4$ mixture, but not in the $H_2O$:$NH_3$:$CO_2$ mixture, while the TPD was terminated at lower temperatures in the other experiments. The carrier of the peak must therefore contain a $CH_x$ group. In the $NH_3$:$CO_2$:$CH_4$, it is present for all investigated $m/z$, including $m/z$=60 and 61. The high desorption temperature suggests a compound which exists as a salt in the ice. There is no infrared features left in the $NH_3$-free mixture above 200 K or in the $CH_4$:$NH_3$ mixture above 150 K and thus the molecule must contain nitrogen and a $CO_x$ group. The strong $m/z$=43, 45 and 46 peaks are indicative of $CH_2COH$ and COOH functional groups. Glycine $NH_2CH_2COOH$ and its structural isomer $CH_3NHCOOH$ ($CH_2COOH$ = 59 amu, NHCOOH = 60 amu, $CH_2COH$/NHCO = 43 amu, COOH=45 amu) are thus the most probable carriers though additional experiments, which include $m/z$=75 are needed to confirm.

A second molecule, which does not contain a $CH_x$ group, also desorbs around this temperature, since there is a desorption peak present at 225 K in the $H_2O$:$NH_3$:$CO_2$ mixture, consisting of $m/z$=45, 46, 43, 29, 27 and 31, but no 59, 60 or 61. $NH_2CHO$ fits this mass pattern, but a new $CO_2$:$NH_3$ experiment is required to test whether the desorption is present there as well. HCOOH in its salt form is another option, which explains some of the observed mass signals.

The next desorption peak, working backwards, is at 215 K and contains $m/z$=61, but not 59 or 60 in both the $H_2O$:$NH_3$:$CO_2$ and $NH_3$:$CO_2$:$CH_4$ mixtures. $m/z$=29 and 45 are also prominent. This is indicative of $NH_2COOH$ desorption ($NH_2COOH$ = 61 amu, COOH = 45 amu, COH = 29 amu).

The desorption peak at 195 K is the first to be investigated that is certainly

present in the astrophysical ice equivalent in the bottom panel in Figs. 1.22–1.24. It is also apparent in the $NH_3$:$CO_2$:$CH_4$ experiment with $m/z$=60, but in no other experiments. The absence in the $H_2O$:$NH_3$:$CO_2$ ice mixture is indicative of the molecule containing a $CH_x$ group, while the absence in the N-free ice mixture advocates a molecule containing nitrogen or an acid, which requires the presence of $NH_3$ to exist in ion form and thus desorb at this high temperature. These facts and the mass pattern fits $CH_3COOH$ and no other considered species.

$H_2O$ desorbs at ~145 K. This is accompanied with significant co-desorption of $m/z \leq 46$ in the astrophycial ice equivalent and in the $H_2O$:$CO_2$:$CH_4$ ice mixture, though the mass signals are different. In the astrophysical ice the $m/z$=45 signal is stronger than the $m/z$=43 signal, while the relation is the opposite in the nitrogen free mixture. Both peaks have multiple possible carriers, but the $H_2O$:$CO_2$:$CH_4$ peak must be dominated by a $C_2H_xO$ type species, while the peak in the astrophysical ice equivalent has a main carrier with a $CO_2$-group such as HCOOH.

The astrophysical ice equivalent and the $CH_4$:$NH_3$ ice mixture contain a peak at ~120 K. The lack of any $m/z$ above 27 suggests that HCN is the carrier – HCN desorbs with $NH_3$ in the $NH_3$:$CH_4$ mixture from the RAIRS. Next, a desorption peak at 110 K is most obvious in the $CH_4$:$NH_3$ ice mixture and its mass pattern with $m/z$=27–31 makes its assignment to $CH_3NH_2$ secure.

There is no co-desorption with $NH_3$ in the astrophysical ice equivalent. The next peak at ~76 K is due to co-desorption with $CO_2$, which contains no obvious evidence for desorption of complex species. Finally the main $C_2H_4$/6 desorption peak at ~62 is present in all $CH_4$ containing ice mixtures.

There is no separate desorption peak for HNCO in any of the experiments, which is at first glance surprising since $OCN^-$ is formed according to the RAIR spectra. Also according to the RAIR spectra, $OCN^-$ starts to desorb around 200 K, and this temperature region does contain $m/z$ signals of 28, 26 and 43. $OCN^-$/HNCO must thus desorb together with other species at this temperature. It probably explains the strong $m/z$=43 signal at this time; while $NH_2CH_2COOH$ may contribute to $m/z$=43, a rather awkward dissociation is required to form it and OCN is a more likely main contributer.

The (tentative) assignments of all desorption peaks are summarized in Table 1.4. TPD experiments following ice photolysis thus provide ample evidence for a complex $NH_3$ based chemistry in $NH_3$-containing ice mixtures up to the formation of simple amino acids. TPD curves provide little quantitative information, however and no information on when these species form during photolysis.

The TPD curves suggest that inspecting difference spectra from before and af-

Table 1.4. The TPD detected species in key ice mixtures with $H_2O$:$CO_2$:$CH_4$:$NH_3$.

| Temp. (K) | $m/z$ | Assignment |
|---|---|---|
| 62 | 27, 30, 29 | $C_2H_4$, $C_2H_6$ |
| 76 | varied | $CO_2$ co-desorption |
| 90 | varied | $NH_3$ co-desorption |
| 110 | 31, 29, 27 | $CH_3NH_2$ |
| 120 | 27 | HCN |
| 145 | varied | $H_2O$ co-desorption |
| 195 | 45, 43, 47, 60 | $CH_3COOH$ ion |
| 215 | 61, 45, 46, 31 | $NH_2COOH$ ion |
| 225 | 45, 43, 46 | $NH_2CHO$ (+HCOOH) ion |
| 230 | 60, 59, 45, 43, 46 | $NH_2CH_2COOH$+$CH_3NHCOOH$ ions (+HNCO) |

[a]Photodestruction crosssection

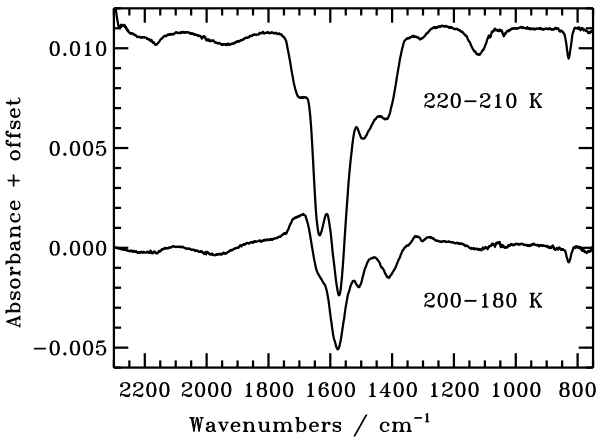


Figure 1.25 Infrared difference spectra of the $NH_3$:$CO_2$:$CH_4$ ice mixture during warm-up, where negative peaks indicate destruction of the carrier in the temperature interval.

ter specific desorption peaks may result in the assignment of some infrared peaks and the derivation of the final abundance of the complex molecule in question. Figure 1.25 shows the difference spectra of the $NH_3$:$CO_2$:$H_2O$ mixture between 220 and 210 K and between 200 and 180 K. According to the TPD curves two different carriers are desorbing at these temperatures. Yet the difference spectra share several bands, indicative of that some of the changes in the RAIRS are due to ice re-structuring, such as dissolving of the salt networks, rather than desorption. Difference spectra during desorption are thus not very useful for $NH_3$:$CO_2$-containing ice mixtures when trying to assign RAIRS features to complex molecules.

Modeling the ice chemistry in the simpler ice mixtures and then using these models to predict the chemistry in astrophysical ice analogues with some quantified chemistry thus remains the best option for quantifying the complete chemistry of the $H_2O$-rich ice phase during star formation.

## 1.4 Discussion

### 1.4.1 Importance of acid-base chemistry in $NH_3$:X ice mixtures

The photodestruction rate of pure $NH_3$ and of $NH_3$ in different ice mixtures differs by factor of four different after a low fluence and by an order of magnitude after an equivalent photon exposure to a million years in a cloud core, i.e. $\sim 3 \times 10^{17}$ photons cm$^{-2}$ Shen et al. (2004). In contrast the $CH_4$ photodissocation rate increases by at most 50% between the pure ice and a similar set of ice mixtures as investigated for $NH_3$.

There are a number of processes that can affect the effective photodissociation cross sections in ices of which the diffusion rates of radicals and as been shown to be important previously (Chapter 10). The diffusion rate can be increased by increasing the ice temperature and decreased by trapping the volatile molecule, e.g. $NH_3$, in a less volatile ice such as $H_2O$. This may explain why the $NH_3$ photodissociation cross section is increased in the $H_2O$:$NH_3$ 4:1 mixture but not in the 1:1 mixture. A similar effect would be expected for $CH_4$. This is not observed, but may be due to that the highest $H_2O$ concentration investigated is $H_2O$:$CH_4$ 2:1 and a 5:1 experiment is required to investigate this further.

The increased photodestruction rate of $NH_3$ in the $H_2O$ ice may also be due to a photo-induced acid-base chemistry where $H_2O$ or a $H_2O$:$NH_3$ photoproduct acts as a weak acid. Acid-base chemistry is the only explanation for the extremely efficient indirect photodestruction of $NH_3$ in a $CO_2$ ice mixture. There

$NH_3$ must be lost both by photodissociation and by proton transfer from photoproducts, such as HCOOH and $H_2CO_3$, to form $NH_4^+$. Acid base chemistry in $NH_3$ and $CO_2$ containing ices also explains the high desorption temperatures of several of the complex molecules, e.g. $NH_2COOH$, $CH_3COOH$ and possibly $NH_2CH_2COOH$/$CH_3NHCOOH$.

The impact on the chemical pathways of this proton transfer is not clear. The tentatively detected complex molecules in the $NH_3$:$CO_2$:X mixtures can all be qualitatively explained by radical-radical reactions, e.g. $NH_2$+$CH_2$+COOH to form $NH_2CH_2COOH$, followed by proton loss to $NH_3$ to form $NH_4^+$. This indicates the the acid-base chemistry does not effect the formation pathways of species, but only the final form of the products and therefore their desorption temperatures.

### 1.4.2 Photodissoication branching ratios

$H_2O$, $CH_4$ and $NH_3$ all photodissociate through the loss of one or multiple hydrogen atoms or a hydrogen molecule, while $CO_2$ exclusively photodissociates into CO+O in the gas phase (van Dishoeck 1988). The $H_2O$ and $NH_3$ photodissociation branching ratios cannot be quantified in the pure ices because of the lack of secure product detections and band strengths. Their gas phase values are however well known and should be valid in the solid state as well. The gas phase $CH_4$ photodissociation branching ratio into $CH_3$ and $CH_2$ is more controversial and experiments have suggest values between 5:1 and 1:1 (Romanzin et al. 2008).

Following $CH_4$ photolysis in the pure ice, both $C_2H_6$ and $C_2H_4$ are detected. The growth curve of $C_2H_4$ contains a small fluence delay, but it is not large enough to infer that $C_2H_4$ is a second generation product as e.g. $CH_3CH_2OH$ seems to be in the $CH_4$:$H_2O$ ice. Thus the initial growth of both $C_2H_4$ and $C_2H_6$ is assumed to be caused by $CH_3$+$CH_3$ and $CH_2$+$CH_2$ radical reactions. Further assuming that the diffusion barriers of $CH_3$ and $CH_2$ are comparable, the $CH_4$ branching ratio can be constrained from the initial $C_2H_6$ and $C_2H_4$ production rate, which is ~9:1. Since each reaction requires two radicals, the dissociation branching ratio is inferred to be ~3:1.

The product ratios during UV irradiation will also depend on the relative radical diffusion barriers. Quantifying these barriers requires, however, a model that simultaneously considers all possible reactions pathways.

### 1.4.3 Radical diffusion: dependence on $H_2O$ content

Diffusion data can also be extracted by monitoring the further formation of complex molecules during warm-up after the UV lamp has been turned off. This is most obvious when comparing the $CH_3OH$ and $CH_3CHO$ formation in a $H_2O$-poor and a $H_2O$-rich $H_2O$:$CH_4$ ice mixture during warm-up, following irradiation at 20 K. In the $H_2O$-poor ice mixture $CH_3OH$ forms during warm-up, but almost no $CH_3CHO$. In the $H_2O$-rich ice the situation is the opposite. In both ices more OH than CHO radicals are expected to form, since OH is a direct photodissociation product of $H_2O$. The growth of $CH_3OH$ in the $H_2O$-poor ice mixture, where diffusion is fast, is thus expected. The enhanced growth of $CH_3CHO$ in the $H_2O$-rich ice is best explained by a slower diffusion rate of OH in this ice mixture, because of the hydrogen-bonding environment, which allows the more volatile CHO radical to react with the available $CH_3$ radicals before OH diffusion becomes possible. While branching ratios can be directly extrapolated from simpler to more complex ice mixtures, it is clear that adding $H_2O$ may change the relative diffusion pattern of the involved radicals significantly and this must be further investigated as outlined below.

### 1.4.4 Radical-radical versus radical-molecule reactions

The CHO radical belongs to the set of species in the considered reaction schemes which form from hydrogenation and oxygenation of molecules rather than radicals, i.e. CO+H, though photodissociation pathways from other molecules are possible as well. The formation of $CO_3$ and $O_3$ in the $CO_2$ ices are other examples as is the tentative evidence for HCOOH formation. Hydrogenation of CO is possible for thermalized hydrogen atoms, while hydrogenation of $CO_2$ is not (Watanabe et al. 2000; Bisschop et al. 2007a). The definite formation of $CO_3$ from $CO_2$+O shows that atom addition to $CO_2$ is possible for at least energetic atoms – whether the O needs to be energetic to react with $CO_2$ should be tested through irradiation of matrix-isolated $CO_2$ followed by warm-up. $CO_2$ hydrogenation may thus be important for energetic hydrogen atoms and HCOOH may form from $CO_2$ + H* + H.

The order of magnitude decrease in $CO_3$ and $O_3$ formation in the ice mixtures compared to the pure $CO_2$ ice and the far smaller effect on CO production demonstrates that radicals are preferentially hydrogenated in ice mixtures of molecules and radicals, in agreement with Hasegawa et al. (1992). A quantitative measurement of this effect would be possible if the relative production rate of HCOOH and $H_2CO_3$ could be determined under some specific conditions and this is being

pursued.

### 1.4.5 Routes to complex organics in space

Chapter 10 showed that photolysis of $CH_3OH$ and CO:$CH_3OH$ ices result in the formation of all common C, O and H bearing complex organic species observed in star forming regions. Several of the same species form abundantly, i.e. a few percent with respect to $CH_4$, during photolysis of $H_2O$:$CO_2$:$CH_4$ ice mixtures as well. The dominating formation pathway of e.g. $CH_3CHO$ will therefore depend on 1) the initial ice abundances and 2) the efficiency of ice mixing during warm-up. Other complex molecules, such as $(CH_2OH)_2$, are still expected to form solely in the $CH_3OH$:CO ice phase.

The N-containing organic species probably require $NH_3$ or XCN to form (a minor route through $N_2$ photolysis cannot be excluded) and their formation paths should be possible to predict from the experiments on $H_2O$-rich ices, without simultaneous consideration of the chemistry in the CO:$CH_3OH$ ice phase.

The pure and binary ice experiments, where the product formation is quite well understood, produce complex photoproducts in accordance with simple radical-radical and radical-molecule reaction schemes. The same complex molecules seem to form in the astrophysical ice analogue and in the binary ice mixtures it can be thought of as being composed of. There is however no simple pattern of how the formation rates of these complex molecules change between the binary ice mixtures and the analogue, and they do change by up to an orde rof magnitude. Some of the observed differences are due to the impact of $H_2O$ on the diffusion of radicals, which will be better understood once new $H_2O$-rich ice mixtures experiments are investigated. To quantitatively test whether the analogue chemistry is consistent with predictions from the binary ice mixtures requires, however, a complete model of the chemistry of both the binary and the analogue mixtures. Such a model should preferentially be calibrated against the better understood chemistry in the simple ice mixtures and then model the analogue based on this calibration. The predicted chemistry can then be compared quantitatively with the growth curves in the analogue and qualitatively with the results from the TPD experiments.

Without such model predictions there can be no quantitative astrophysical predictions on the photochemistry in the $H_2O$-rich ice phase. It is however clear that substantial amounts of amino acids and amino acid-like compounds can form in $NH_3$ and $CO_2$ containing ices. The experiments also show that these large molecules form during irradiation of astrophysically plausible ice mixtures at 20 K or due to diffusion of formed radicals during warm-up of the same ices to at most

200 K. Room temperature induced reactions are therefore not required to form such complex molecules, which is promising for the formation of large molecules in ices in space.

The presence of N-containing complex molecules in the ice in ionic form will result in desorption at higher temperatures compared to e.g. $H_2O$ or even $(CH_2OH)_2$. This may explain the lack of glycine detections so far – it is likely to only exist very close to the protostar in the gas phase.

### 1.4.6 Future experiments

To accurately predict the complex chemistry in astrophysically realistic ice mixtures would benefit from a number of additional experiments focusing on the impact of $H_2O$ on the diffusion of radicals and molecules, especially $CH_3$, $CH_2$, $NH_2$, NH, CO and HCO. This can be achieved by quantifying the changes in the chemistry of the binary mixtures investigated here when they are mixed with five times as much $H_2O$ and then irradiated at 2–3 temperatures, e.g. 20, 40 and 60 K.

Analyzing these new experiments similarly to the approach above would directly constrain more relative diffusion barriers from the changing product branching ratios, though a large quantitative model is required to extract all information contained in such a set of experiments.

These experiments would also constrain the mechanism behind the increasing photodestruction cross section of $NH_3$ in a $H_2O$-dominated matrix. If it is due to trapping of radicals in the ice and thus hindering recombination to form $NH_3$, increasing the temperature should lower the photodestruction rate. If it is instead due to acid-base chemistry between $NH_3$ and $H_2O$-photoproducts, the photodestruction rate should increase or remain unchanged in a warmer ice.

## 1.5 Conclusions

There is no doubt that complex nitrogen-bearing molecules can form through photochemistry in the $H_2O$-rich ice observed towards protostars. The experimental quantification of this formation process is non-trivial because of overlapping infrared spectral features in astrophysical ice mixtures analogues. This difficulty was addressed by combining the quantification of a small set of photolysis products in a range of pure ices, binary ice mixtures and more complex astrophysical ice analogues, and TPD experiments constraining the formation of more complex species. The main findings from this approach are enumerated below.

1. The product ratio of $C_2H_6$ and $C_2H_4$ in pure $CH_4$ ice implies a $CH_4$ photodissociation branching ratio of $CH_3$:$CH_2$ of 3:1.

2. In binary $CH_4$:$NH_3$/$H_2O$/$CO_2$ and $NH_3$:$CO_2$ ice mixtures the formation curves of $C_2H_6$, $CH_3NH_2$ and $CH_3OH$ are consistent with formation from two first generation radicals, while HCN, $CH_3CH_2OH$, $CH_3CHO$ and $OCN^-$ formation requires several reaction steps. This is consistent with reaction schemes, where products form from radical-radical and radical-molecules reactions, and radicals are produced both from photodissociation of the original ice constituents and through photodissociation of first-generation photoproducts.

3. Increasing the $H_2O$ concentration in the ice increases the diffusion barriers of hydrogen-bonding radicals, which affects the chemical evolution of the ice.

4. $NH_3$ ice is both destroyed directly from UV photons through photodissociation and indirectly through proton transfer with other photoproducts. In $CO_2$ containing ices, the indirect acid-base $NH_3$ destruction path is up to an order of magnitude more important.

5. The most abundant photoproducts in the binary ices are also detected upon irradiation of a $H_2O$:$CO_2$:$NH_3$:$CH_4$ 100:20:12:8 astrophysical ice analogue. The formation rates are however different compared to most binary ices because of acid-base chemistry and the different diffusion pattern in $H_2O$-rich and $H_2O$-poor ices.

6. TPD experiments of tertiary ice mixtures shows that glycine can form already at low temperatures in ices containing $CO_2$:$NH_3$:$CH_4$. Other detected photoproducts are $NH_2CHO$, $CH_3COOH$ and $NH_2COOH$. All exist in salt form because of proton transfer with $NH_3$, which results in higher desorption temperatures than e.g. $H_2O$ ice.

The results suggest that the information from the pure and binary ice mixture experiments can be used to model the chemistry in astrophysical ice analogues both in the laboratory and under astrophysical conditions. Quantifying the complex N-bearing ice chemistry during star and planet formation is thus within reach.

## References

Allamandola, L. J., Sandford, S. A., & Valero, G. J. 1988, Icarus, 76, 225
Altwegg, K., Balsiger, H., & Geiss, J. 1999, Space Science Reviews, 90, 3
Belloche, A., Garrod, R. T., Müller, H. S. P., et al. 2009, A&A, 499, 215
Belloche, A., Menten, K. M., Comito, C., et al. 2008, A&A, 482, 179
Bergin, E. A., Alves, J., Huard, T., & Lada, C. J. 2002, ApJL, 570, L101
Bernstein, M. P., Dworkin, J. P., Sandford, S. A., Cooper, G. W., & Allamandola, L. J. 2002, Nature, 416, 401
Bernstein, M. P., Sandford, S. A., Allamandola, L. J., Chang, S., & Scharberg, M. A. 1995, ApJ, 454, 327
Bisschop, S. E., Fuchs, G. W., van Dishoeck, E. F., & Linnartz, H. 2007a, A&A, 474, 1061
Bisschop, S. E., Jørgensen, J. K., van Dishoeck, E. F., & de Wachter, E. B. M. 2007b, A&A, 465, 913
Blau, E. J., Hochheimer, B. F., & Unger, H. J. 1961, J. Chem. Phys., 34, 1060
Brewer, L. & Wang, J. L.-F. 1972, J. Chem Phys., 56, 759
Ceccarelli, C., Loinard, L., Castets, A., Faure, A., & Lefloch, B. 2000, A&A, 362, 1122
Combes, F., Q-Rieu, N., & Wlodarczak, G. 1996, A&A, 308, 618
Cottin, H., Moore, M. H., & Bénilan, Y. 2003, ApJ, 590, 874
Crovisier, J., Bockelée-Morvan, D., Colom, P., et al. 2004, A&A, 418, 1141
D'Hendecourt, L. B. & Allamandola, L. J. 1986, A&AS, 64, 453
Elsila, J. E., Dworkin, J. P., Bernstein, M. P., Martin, M. P., & Sandford, S. A. 2007, ApJ, 660, 911
Engel, M. H. & Macko, S. A. 1997, Nature, 389, 265
Garrod, R. T. & Herbst, E. 2006, A&A, 457, 927
Garrod, R. T., Weaver, S. L. W., & Herbst, E. 2008, ApJ, 682, 283
Gerakines, P. A., Moore, M. H., & Hudson, R. L. 2004, Icarus, 170, 202
Gerakines, P. A., Schutte, W. A., & Ehrenfreund, P. 1996, A&A, 312, 289
Gerakines, P. A., Schutte, W. A., Greenberg, J. M., & van Dishoeck, E. F. 1995, A&A, 296, 810
Gibb, E. L., Whittet, D. C. B., Boogert, A. C. A., & Tielens, A. G. G. M. 2004, ApJS, 151, 35
Greenberg, J. M. 1983, Advances in Space Research, 3, 19
Grim, R. J. A., Greenberg, J. M., de Groot, M. S., et al. 1989, A&AS, 78, 161
Hagen, W., Allamandola, L. J., & Greenberg, J. M. 1979, Ap&SS, 65, 215

Hasegawa, T. I., Herbst, E., & Leung, C. M. 1992, ApJS, 82, 167
Hiraoka, K., Miyagoshi, T., Takayama, T., Yamamoto, K., & Kihara, Y. 1998, ApJ, 498, 710
Knez, C., Boogert, A. C. A., Pontoppidan, K. M., et al. 2005, ApJ, 635, L145
Lacy, J. H., Faraji, H., Sandford, S. A., & Allamandola, L. J. 1998, ApJ, 501, L105+
Lee, C.-W., Kim, J.-K., Moon, E.-S., Minh, Y. C., & Kang, H. 2009, ApJ, 697, 428
Moore, M. 1991, Spectrochimica Acta Part A: Molecular Spectroscopy, 47, 255
Moore, M. H. & Hudson, R. L. 1998, Icarus, 135, 518
Muñoz Caro, G. M., Meierhenrich, U., Schutte, W. A., Thiemann, W. H.-P., & Greenberg, J. M. 2004, A&A, 413, 209
Muñoz Caro, G. M., Meierhenrich, U. J., Schutte, W. A., et al. 2002, Nature, 416, 403
Muñoz Caro, G. M. & Schutte, W. A. 2003, A&A, 412, 121
Nuevo, M., Chen, Y.-J., Yih, T.-S., et al. 2007, Advances in Space Research, 40, 1628
Öberg, K. I., Linnartz, H., Visser, R., & van Dishoeck, E. F. 2009a, ApJ, 693, 1209
Öberg, K. I., van Dishoeck, E. F., & Linnartz, H. 2009b, A&A, 496, 281
Pearl, J., Ngoh, M., Ospina, M., & Khanna, R. 1991, J. Geophys. Res., 96, 17477
Romanzin, C., Bénilan, Y., Jolly, A., & Gazeau, M.-C. 2008, Advances in Space Research, 42, 2036
Roux, J. A. & Wood, B. E. 1983, J. Opt. Soc. Am., 73, 1181
Schutte, W. A., Allamandola, L. J., & Sandford, S. A. 1993, Icarus, 104, 118
Schutte, W. A. & Khanna, R. K. 2003, A&A, 398, 1049
Shen, C. J., Greenberg, J. M., Schutte, W. A., & van Dishoeck, E. F. 2004, A&A, 415, 203
Thompson, W. & Jacox, M. 2001, JOURNAL OF CHEMICAL PHYSICS, 114, 4846
van Broekhuizen, F. A., Keane, J. V., & Schutte, W. A. 2004, A&A, 415, 425
van Broekhuizen, F. A., Pontoppidan, K. M., Fraser, H. J., & van Dishoeck, E. F. 2005, A&A, 441, 249
van Dishoeck, E. F. 1988, in Rate Coefficients in Astrochemistry. Proceedings of a Conference held in UMIST, Manchester, United Kingdom, September 21-24, 1987. Editors, T.J. Millar, D.A. Williams; Publisher, Kluwer Academic Publishers, Dordrecht, Boston, 1988. ISBN # 90-277-2752-X. LC # QB450

.R38 1988. P. 49, 1988, ed. T. J. Millar & D. A. Williams, 49–+

Visser, R., van Dishoeck, E. F., Doty, S. D., & Dullemond, C. P. 2009, A&A, 495, 881

Watanabe, N., Horii, T., & Kouchi, A. 2000, ApJ, 541, 772

Whittet, D. C. B., Gerakines, P. A., Tielens, A. G. G. M., et al. 1998, ApJ, 498, L159

Woon, D. E. 2002, ApJ, 571, L177